Applied Catalysis B: Environmental 204 (2017) 89–106

Contents lists available at ScienceDirect

Applied Catalysis B: Environmental

journal homepage: www.elsevier.com/locate/apcatb

Effect of Pt addition on sulfur dioxide and water vapor tolerance of Pd-Mn-hexaaluminate catalysts for high-temperature oxidation of methane

S.A. Yashnik[a,*], Yu.A. Chesalov[a,b], A.V. Ishchenko[a], V.V. Kaichev[a,b], Z.R. Ismagilov[a,c]

[a] Boreskov Institute of Catalysis, Lavrentieva Ave. 5, Novosibirsk, 630090, Russia
[b] Novosibirsk State University, Pirogova Str. 2, Novosibirsk, 630090, Russia
[c] Institute of Coal Chemistry and Material Science, Sovetskiy Ave. 18, Kemerovo, 650000, Russia

ARTICLE INFO

Article history:
Received 10 June 2016
Received in revised form 21 October 2016
Accepted 10 November 2016
Available online 11 November 2016

Keywords:
Methane oxidation
Mn-hexaaluminate
Pt-catalyst
Pd-catalyst
Sulfur-resistance

ABSTRACT

An effect of Pt addition to improve the catalytic performance of Pd-modified Mn-hexaaluminate in the high-temperature oxidation of methane, especially in SO_2 and water presence, has been studied. X-ray diffraction, high-resolution transmission electron microscopy, X-ray photoelectron spectroscopy, thermogravimetry and differential thermal analysis were used for the characterization of fresh and spent catalysts. Temperature-programmed reduction by hydrogen was employed to study the redox properties of the catalysts. Four high-temperature tests (at 670 °C) of the methane oxidation were applied to reveal the water and sulfur resistance of the catalysts: 1) dry methane-air feed; 2) wet methane-air feed containing 3 wt% of water vapor; 3) methane-air feed containing 1000 ppm of SO_2; and 4) wet methane-air feed with 1000 ppm of SO_2. The Pt-doped Pd-Mn-hexaaluminate catalyst with the atomic ratio of Pt/Pd < 0.3 has been shown to possess the highest catalytic activity in the oxidation of methane, high water and sulfur tolerance, and reducibility by hydrogen as compared to the monometallic Pd-Mn-hexaaluminate catalyst and the bimetallic catalysts with Pt/Pd > 0.5. From the formal kinetic data of the oxidation of methane on the fresh and deactivated catalysts, we assumed that deactivation of the catalysts is due to a decrease in the amount of catalytically active sites in the bimetallic 0.33Pt-0.67Pd(0.27)/$MnLaAl_{11}O_{19}$ catalyst and a change in the state of active component in the other catalysts. Their oxidation ability and redox behavior were shown to be associated with the highly dispersed PdO particles, a PdO layer (3–5 nm) covering the metal palladium particles as well as the Mn^{3+}-enriched $MnLaAl_{11}O_{19}$. The improved water and sulfur resistance is found to correlate with the presence of particles of PtPd alloy, with its fraction not exceeding 50%.

1. Introduction

It is reliably ascertained that Pd-based catalysts feature higher catalytic activity in the oxidation of methane as compared with other catalysts based on supported noble metals [1–3]. Therefore, Pd-based materials are the most promising catalysts for the gas-turbine plants (GTP) which use natural gas as a fuel [4–9]. Some companies, such as Catalytica (USA) and Kawasaki Heavy Industries (Japan), have developed Pd-based catalysts to the level close to industrial use in the catalytic gas turbines of high power [10]. However, the reaction ability in the oxidation of methane and stability of the majority of Pd-based catalysts intended to be used in the catalytic combustion chamber (CCC) decrease in the presence of water vapors and SO_2 [11–23]. It should be noted that water forms as a product of burning of hydrocarbons, and sulfur dioxide is a result of oxidation of hydrogen sulfide admixed to natural gas in quite a significant amount (1–2 vol.%).

The degree of deactivating influence of water is supposed to depend on the reaction temperature [12–15], the rate of gas flow [13], the concentration of water in the reaction feed [16,17], and other parameters of the methane oxidation process. For PdO-supported catalysts based on ZrO_2, this influence manifests itself to the highest degree at temperatures below 450 °C in the pulse mode and below 650 °C in the flow mode [12]. Deactivation of PdO/ZrO_2 is related to the slow desorption of water from the catalyst surface at low temperatures [12,13]. At the same time, no inhibiting effect of water is observed for the catalysts containing palladium in the form of metal particles [13]. Burch et al. showed that PdO-containing cat-

* Corresponding author.
E-mail address: yashnik@catalysis.ru (S.A. Yashnik).

http://dx.doi.org/10.1016/j.apcatb.2016.11.018
0926-3373/

alysts based on Al_2O_3 are irreversibly deactivated in the presence of water at a temperature of 300 °C and lower as a result of hydroxylation of PdO surface to inactive particles of $Pd(OH)_2$ [11,14,15], and at a temperature of 450 °C and higher the deactivation is insignificant [14]. Ribeiro et al. [16] believe that the deactivation of PdO supported catalysts based on Al_2O_3 and ZrO_2 by the products of reaction (H_2O and CO_2) is related to the dispersion of the large particles of PdO to the stable highly-dispersed phase of PdO, covering the support by a monolayer and having a strong interaction with the support. Another reason for the deactivation of PdO-containing catalysts by water vapors is a low rate of methane activation [13], particularly at high temperatures.

The fast deactivation of Pd-containing catalysts on non-sulfating supports, for instance, SiO_2, is being linked to the selective adsorption of sulfur dioxide on highly active particles of PdO, resulting in their transformation to less active PdO-SO_x [18–20]. The sulfatation of palladium is confirmed by infrared spectroscopy data [20] and kinetic data indicating a drop in the number of sites active in the oxidation of methane [18,21]. As a rule, palladium sulfate decomposes at a temperature above 600 °C [18,24]. In the case of Pd on sulfating supports, such as Al_2O_3 and ZrO_2 [18,20], the deactivation occurs at a slower rate, since SO_x adsorbs both on PdO and the support [18,21–23]. It is stated that PdO promotes the sulfatation of alumina under oxidizing conditions [19]. The sulfatation of PdO/Al_2O_3 is partially reversible at a temperature of 420 °C [22,25,26] and completely reversible at 520 °C [22]. The surface and bulk aluminum sulfates in the deactivated PdO/Al_2O_3 were detected by XPS [21] and FTIR [23]. In addition, some experiments showed a decrease in the activation energy from the value corresponding to the kinetic control of the oxidation of methane to the values of the inner diffusion mode [18,21], which also indicates the sulfatation of alumina. Therefore, the tendency of the catalyst to be deactivated with sulfur dioxide and to regenerate depends on the support nature, namely, on its ability to form sulfate, which increases in the row from non-sulfating supports (SiO_2, ZrO_2-SiO_2) to sulfating ones (Al_2O_3, ZrO_2). The deactivation of Pd-based catalysts with sulfur dioxide is accelerated by the presence of water vapor [23,26].

It is considered to be proven that Pt-based catalysts surpass Pd-based catalysts in their resistance to the deactivation with sulfur dioxide [18,19,22,24], because platinum oxide does not adsorb SO_2 [18]. Consequently, in order to increase the sulfur-resistance of Pd-based catalysts they can be modified by adding platinum. This method is used successfully when developing the catalysts for purification of exhaust of motor vehicles [24,27,28] exploited, however, at a lower temperature (below 900 °C) as compared with CCC GTP. A positive effect of Pt was also observed for the hydrodesulfurization of Pd-based catalysts [29,30], which work under reducing conditions. There are examples of an increase in the sulfur-resistance of bimetallic PtPd-catalysts in the oxidation of methane; however, this effect manifests itself for the catalysts subjected to previous activation in the reducing medium with the following sulfatation [31]. Corro et al. [31] believe that the metal particles of Pt formed in the reducing conditions are necessary to prevent SO_2 adsorption on palladium and deactivation of bimetallic PtPd-catalysts.

There are several examples in the literature describing the bimetallic catalysts based on pure Al_2O_3 [32–39] and on Al_2O_3 modified by ZrO_2 [36], which demonstrate high thermal stability in the oxidation of methane, however, there is no information on the thermal stability of Pd-containing catalysts based on Mn-hexaaluminates and their resistance to the deactivation in the presence of water vapor and sulfur-containing compounds, as well as on the influence of platinum addition on the mentioned characteristics. In addition, the majority of the known catalysts have high loadings of noble metals (no less than 4 wt%), which results in a significant rise in price of the catalytic combustion chambers.

In this work we studied an effect of Pt addition to improve the catalytic performance of high-temperature Pd-modified Mn-hexaaluminate in the oxidation of methane, especially in SO_2 and water presence. We considered the catalysts with the total content of noble metals of 1 wt%. In order to significantly lower the content of noble metals in the catalysts, we used the effect of non-additive increase in the activity of Mn-hexaaluminates in the high-temperature methane oxidation after their modification by Pd [40,41], resulting in a decrease in the light-off temperature. Mn-hexaaluminate maintains the stable oxidation of methane in the catalytic combustion chamber at temperatures of 670–900 °C [7], ensuring 99.9% conversion of methane and non-toxicity of the waste gas (no more than 10 ppm CO) starting with the Pd content of 0.8–1.0 wt% [6,8]. The redox properties, particle morphology, structure and the state of active component of the fresh and spent PtPd-modified Mn-hexaaluminates were examined in order to find a reason of their methane oxidation efficiency in the SO_2 and water presence.

2. Experimental

2.1. Catalyst preparation

A ring-shaped granulated alumina containing 60% of γ-Al_2O_3 and 40% of χ-Al_2O_3 with the specific surface area 284 m^2/g and the pore volume 0.49 cm^3/g was used for preparation of the Mn-hexaaluminate precursor. The Mn-hexaaluminate precursor and the catalysts with $MnLaAl_{11}O_{19}$ phase were prepared according to the procedure described elsewhere [40,41]. Thereto, the granulated alumina was impregnated by lanthanum and manganese nitrate solutions followed by drying at 110 °C for 2 h and calcination in air at 400 °C for 4 h. The La_2O_3 loading was 11.7–12.5 wt%, and the MnO_2 loading was 11.2 wt%. The sample calcined at 400 °C (called Mn-hexaaluminate precursor) had the specific surface area and the pore volume equal to 98–105 m^2/g and 0.36 cm^3/g, respectively, with prevalent pore diameters of 8.5–13.5 nm. For formation of Mn-hexaaluminate phase $MnLaAl_{11}O_{19}$, the sample was calcined at 1000 °C for 4 h. The specific surface area was approximately 43–44 m^2/g, the pore volume was 0.24–0.25 cm^3/g, and the prevalent pore size was 17–22 nm.

The low-temperature precursor of Mn-hexaaluminate was doped with Pd and Pt by incipient wetness impregnation with a combined solution of palladium/platinum nitrates followed by calcination at 1000 °C for 4 h. The total content of noble metals was 1.0 wt%, the atomic ratio of Pt to Pd was varied in a range of 0.1–1.1.

The catalysts are referred to as xPt-yPd(w)/$MnLaAl_{11}O_{19}$, where x and y is Pt and Pd loading (wt%), respectively, w is the atomic ratio of Pt to Pd, $MnLaAl_{11}O_{19}$ is a support.

2.2. Catalyst characterization

The catalysts were characterized by elemental analysis, X-ray photoelectron spectroscopy (XPS), Fourier transform infrared spectroscopy (FTIR), high-resolution transmission electron microscopy (HRTEM), N_2 adsorption, thermogravimetry and differential thermal analysis (TG–DTA), X-ray diffraction (XRD), and temperature-programmed reduction by hydrogen (H_2-TPR) techniques. The concentrations of Mn and La were determined by atomic absorption spectroscopy with inductively coupled plasma (AAS-ICP) using a BLYRD analyzer. The loadings of Pt and Pd were determined by X-ray fluorescence analysis using an ARL spectrometer with an Rh-anode X-ray tube. The specific surface area (S_{BET}) was calculated with the Brunauer–Emmett–Teller (BET) method using nitrogen

adsorption isotherms measured at the liquid nitrogen temperature with an automatic Micromeritics ASAP 2400 sorptometer. The total pore volumes (V_Σ) and the macropore size were determined by mercury porosimetry using a Porosiger-9300 instrument.

Powder XRD measurements were performed on a HZG-4C diffractometer using the monochromatic CuK_α (λ = 1.5418 Å) radiation. The XRD patterns were recorded in a continuous mode in the 2θ range from 10° to 70° with 1°/min scanning rate. The phase composition was identified using the JCPDS database (PCPDF Win. Ver 1.30, JCPDS ICDD, Swarthmore, PA, USA, 1997).

HRTEM images were obtained using a JEOL JEM-2010 electron microscope with a lattice-fringe resolution of 0.14 nm at the accelerating voltage of 200 kV. The high-resolution images of periodic structures were analyzed by the Fourier method. Local energy-dispersive X-ray analysis (EDXA) was carried out using an EDX spectrometer (EDAX Co.) equipped with a Si (Li) detector which provided the spatial resolution of 10 nm for the HRTEM images and 100 μm in the integrated mode. Before measurements the samples were prepared by ultrasonicating a small quantity of the powder in ethanol for several minutes. The resultant slurry was then deposited on perforated carbon films mounted on copper grids.

XPS measurements were performed on an X-ray photoelectron spectrometer (SPECS Surface Nano Analysis GmbH, Germany) equipped with an X-ray source XR-50 with a twin Al/Mg anode and a hemispherical electron energy analyzer PHOIBOS-150. The core-level spectra were obtained using the non-monochromatic Mg$K\alpha$ (hn = 1253.6 eV) radiation under ultrahigh vacuum conditions. Relative concentrations of elements within the analysis area were determined from the integrated intensities of core-level spectra using the cross-sections according to Scofield [42]. The charge correction was performed by setting the C*1 s* peak at 284.8 eV. The curve-fitting procedure is described in detail elsewhere [43].

IR spectra were recorded on a Cary 660 FTIR spectrometer (Agilent Technologies) within a range of 4000–250 cm^{-1} at a resolution of 4 cm^{-1} in the Attenuated Total Reflectance mode using a Gladi-ATR unit. The spectra of the catalysts were measured without using the diluents.

The thermal analysis was carried out with a NETZSCH STA 449C apparatus in a temperature range from 20 to 1350 °C at the heating rate of 10 °C/min in air. The accuracy of determination of weight losses and temperature was 0.5% and 5%, respectively.

H_2-TPR experiments were carried out using the gas mixture containing 10 vol.% H_2 in Ar with a flow rate of 30 ml/min in a home-made apparatus equipped with a thermal conductivity detector. The temperature was raised from 0 to 900 °C at 10 °C/min rate. Before the H_2-TPR experiments, the samples were first pretreated in oxygen at 500 °C for 30 min and cooled to room temperature, then flushed with an Ar flow. The weight of the samples was 100 mg and the particle size was approximately 250–500 μm. Water produced during the H_2-TPR experiment was removed using a cold trap operated at −70 °C. Calibration for the hydrogen consumption was carried out using the CuO reduction process.

2.3. Catalytic activity tests

The catalysts were tested in the oxidation of methane under conditions typical of Small Gas Turbine Power Plants: the reaction temperature was 670 °C and the feed gas hourly space velocity (GHSV) was 10000 h^{-1}. Gas feed was 5 vol.% CH_4 in air. The coefficient of oxygen excess (α), which was a ratio between oxygen concentration in the gas feed and the stoichiometric amount of oxygen needed for the deep oxidation of methane (10 vol.%O_2/5 vol.%CH_4 = 2/1), was close to 2. After achieving the steady-state value of the CH_4 conversion in the dry methane-air feed, 3 wt% H_2O was introduced in the feed and the CH_4 conversion was measured again. When the CH_4 conversion in the wet feed became steady, the water input was stopped and 1000 ppm SO_2 was added in the feed, the CH_4 conversion was continued to measure. After reaching the stable value of the methane conversion in the SO_2 presence, water was supplied again to the feed and the methane conversion in the presence of water (3 wt%) and sulfur dioxide (1000 ppm) was measured.

To determine the degree of catalyst deactivation in the presence of water vapor and sulfur dioxide, the fresh and deactivated catalysts were studied in the oxidation of methane in the temperature range of 200–700 °C at the space velocity of 10,000 h^{-1}. The methane concentration was 1 vol.% in air, α was 10.

All tests were carried out in a quartz flow reactor placed into a furnace. For the temperature control, a K-type thermocouple inserted in the catalyst bed was used. The granulated catalyst fractionated a grain size 0.5–1.0 mm. The catalyst amount of 1 cm^3 was used in the experiments. To prevent the homogeneous oxidation of methane, the free space of the catalytic reactor was filled with quartz grit with a fractional composition of 1–2 mm.

The reactants and reaction products were analyzed using a gas chromatograph equipped with a thermal conduction detector. A Porapak Q column (i.d. = 3 mm, L = 3 m) was used to separate the reaction products. A molecular sieve 5A column (i.d. = 3 mm, L = 2 m) was used to determine the oxygen concentration. The CH_4 conversion (X_{CH4}, %) was calculated from the experimental concentrations of the reagents and products using the following equation:

$$X = \frac{C^0_{CH4} - C_{CH4}}{C^0_{CH4}} \times 100(\%),$$

where C°_{CH4} is the concentration of methane (vol.%) in the feed, C_{CH4} is the concentration of methane (vol.%) at the reactor outlet. The experimental data were presented as dependences of the methane conversion on temperature.

For the fresh and deactivated catalysts, the pre-exponential factors and the activation energies were estimated from the Arrhenius plot of logarithm of the reaction rate constant against inverse temperature. With this in mind, the reaction rate constant was calculated from the fractional methane conversion at low methane conversion (<25%) assuming pseudo-first reaction order with respect to methane, by using the formula:

$k = -\frac{1}{\tau}\left[\ln(1 - X/100)\right]$, where τ is the space time, defined as the catalyst volume divided by the volumetric feed rate of the reactant.

3. Results and discussion

3.1. Effect of water and SO_x in feed on catalytic performance of Pt-Pd-modified Mn-hexaaluminate

The main source of thermal energy that can be burned in the catalytic combustion chambers of low-power GTP is natural gas. Natural gas contains hydrogen sulfide, sometimes in significant amounts, up to 1–2 vol.%. Under the oxidation conditions, hydrogen sulfide transforms to sulfur dioxide. The oxidation of methane produces water, and its content can vary within the range of 2–10 vol.%. Both sulfur dioxide and water vapor have a deactivating effect on the catalytic properties of Pd-containing catalysts based on Al_2O_3 [11–23].

The influence of water vapor and sulfur dioxide on the catalytic performance of bimetallic Pt-Pd-modified catalysts based on $MnLaAl_{11}O_{19}$ was studied for the catalysts with the Pt/Pd ratio of 0.27 and 1.1, which demonstrated the highest and lowest activity in the oxidation of methane within the dry methane-air mixture with regard to the monometallic Pd-based catalyst [46]. Their resistance to deactivation by water vapor and sulfur we compared with the characteristics of $MnLaAl_{11}O_{19}$ and monometallic Pd-modified

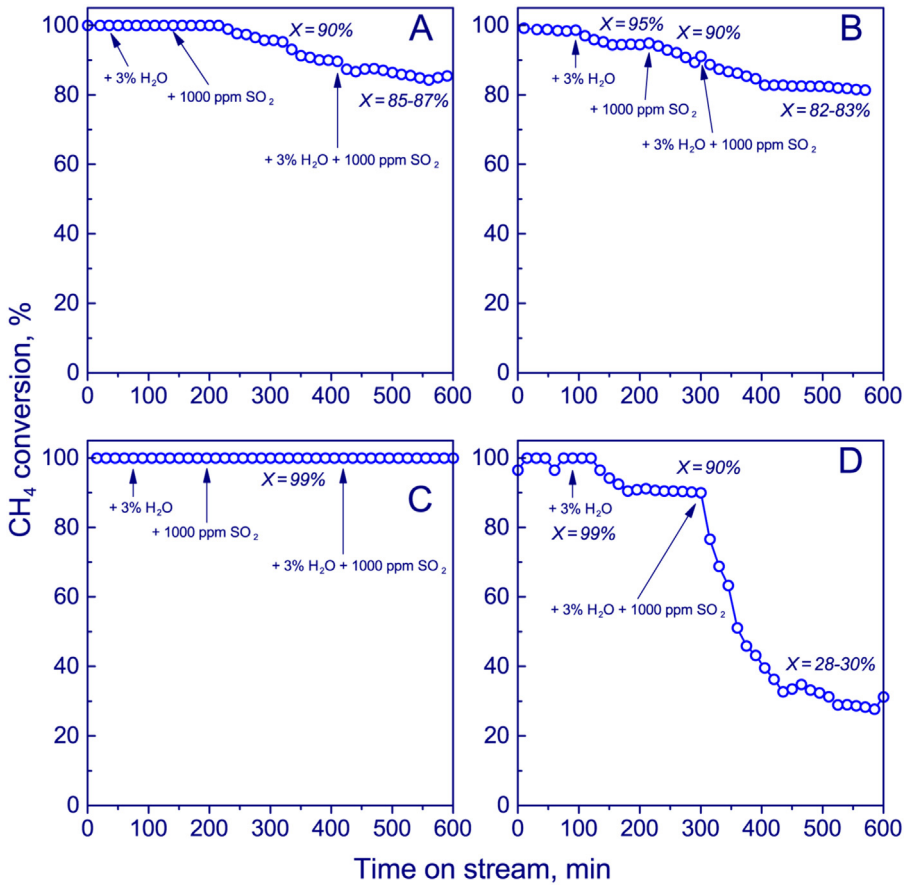

Fig. 1. Methane conversion on $MnLaAl_{11}O_{19}$ (A), 0.82Pd(0)/$MnLaAl_{11}O_{19}$ (B), 0.33Pt-0.67Pd(0.27)/$MnLaAl_{11}O_{19}$ (C), and 0.67Pt-0.33Pd(1.1)/$MnLaAl_{11}O_{19}$ (D) catalysts, calcined at 1000 °C, in dry reactant mixture (5% CH_4, $\alpha = 2$), after addition of water vapor (3 wt%) or/and sulfur dioxide (1000 ppm) to reactant mixture. Temperature in the catalytic bed was 670 °C. GHSV was 10,000 h^{-1}.

catalysts based on $MnLaAl_{11}O_{19}$. The results of the experiments are given in Figs. 1 and 2.

For the catalytic experiments we chose the conditions that are the closest to those realized in the catalytic combustion chambers of low-power GTP, such as a temperature of 670 °C and a gas hourly space velocity of 10,000 h^{-1}. With the indicated GHSV, the oxidation of methane on the monometallic Pd-based catalyst occurs under the kinetic control [5–8]. The preliminary blank experiments, which are carried out with the reactor filled with an inert material, display the methane conversion in dry and wet methane-air feeds as low as 5–8%. These experimental results allow us comparing the catalytic characteristics of bimetallic catalysts of various compositions. As the experimental data presented in Fig. 1 show, all four catalysts at 670 °C and GHSV = 10,000 h^{-1} provide the methane conversion no less than 99% with its oxidation in the dry methane-air mixture. However, the catalysts react differently to the adding of water vapor and SO_2 to the methane-air mixture.

Thus, at 670 °C the sample of Mn-hexaaluminate keeps the methane conversion in the wet reaction feed (3 wt% H_2O) near 99% (Fig. 1A). Whereas Pd-modified Mn-hexaaluminate is subjected to a weak deactivation with water vapor, the methane conversion on the 0.8%Pd(0)/$MnLaAl_{11}O_{19}$ catalyst drops from 99% to 95% after input 3 wt% of water into the methane-air mixture (Fig. 1B). Substitution of 0.33 wt% of palladium in the catalyst with platinum (Pt/Pd = 0.27) results in an increase in stability of the Pd-modified catalyst in the presence of water vapor, the methane conversion reaches 99% both before and after addition of water vapor into the reactant mixture (Fig. 1C). However, an increase in concentration of Pt to 0.67 wt% (Pt/Pd = 1.1) causes a certain decrease in the hydrothermal resistance of the catalyst, in particular, the methane conversion at 670 °C on the 0.67Pt-0.33Pd(1.1)/$MnLaAl_{11}O_{19}$ catalyst was 99% and 90% in the dry and wet methane-air mixture, respectively (Fig. 1D).

Hence, two conclusions can be drawn here. The first is the high resistance of Mn-hexaaluminate to the deactivation by water compared with the Pd-modified catalyst and the bimetallic catalyst with a high Pt-loading. It is due to location of Mn^{3+}/Mn^{2+} cations in the spinel blocks of hexaaluminates [44]. Indeed, the surface hydroxyls formed under water presence in the feed affect weakly the electronic state of Mn^{3+}/Mn^{2+} cations in the support and its catalytic behavior in the oxidation of methane; whereas the Pd-based catalysts form at this conditions an inactive surface Pd-hydroxide [14,39] as well as the hydroxyl accumulation on the support inhibits oxygen exchange between Pd and PdO [45]. Besides, the Mn-cation was found [41] to relocate during the modification of the Mn-hexaaluminate precursor by noble metals; so, an enrichment of catalyst surface by the Mn^{3+} cation taken place at the modification can explain also the change of the catalytic performance of Pd-doped Mn-hexaaluminate in the wet methane-air feed. The low oxidative activity of the high-loaded Pt,Pd-modified catalysts both dry and wet methane-air feeds is likely connected with a strong inhibition effect of Pt on the PdO formation [46], which is completely suppressed at the Pt/Pd ratio equal to 1 [35]. Metallic Pd and Pt/PtO_x are presumed [1–3,11,31] to possess the lower oxidative activity compared with PdO. Secondly, we obtained the range of the Pt/Pd atomic ratios (0.27 and below), in which the bimetallic catalysts based on Mn-hexaaluminate are resistant to the deactivation with water vapor, and it differs somewhat from the data for a PtPd-

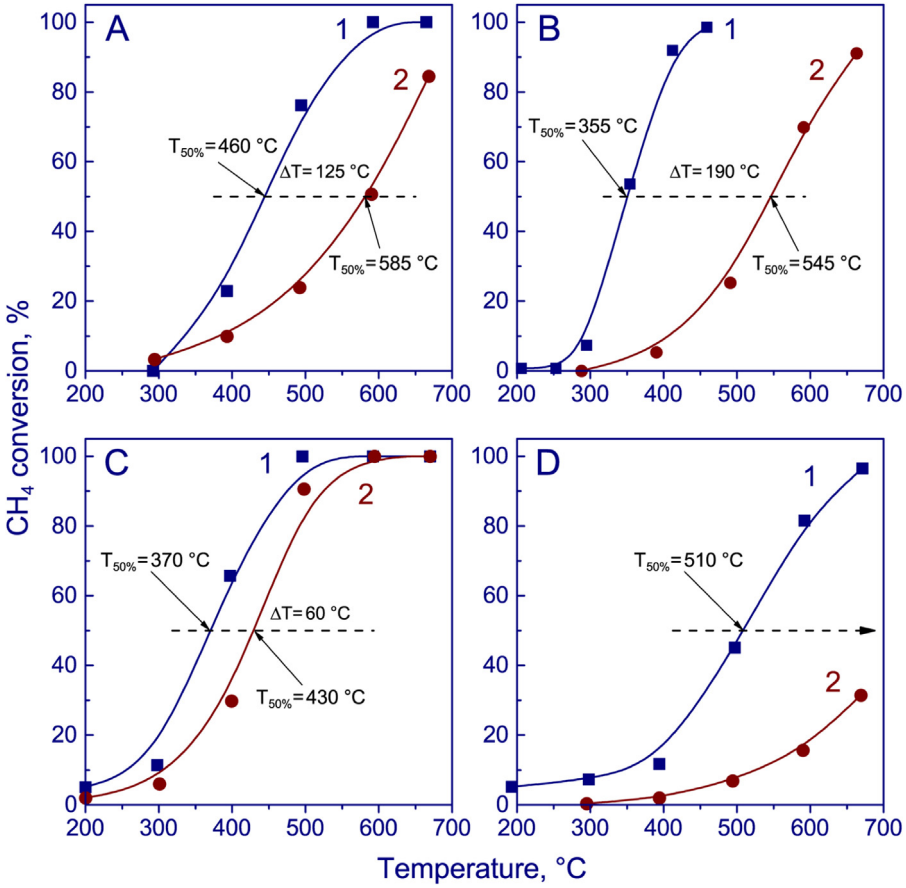

Fig. 2. Temperature dependences of the methane conversion in dry air-methane mixture (1% CH_4, α = 10, GHSV = 10,000 h^{-1}) on the fresh catalyst (curve 1) and the catalyst after testing at 670°C in mixture, containing water vapor and SO_2 (curve 2). $MnLaAl_{11}O_{19}$ (A), 0.82Pd(0)/$MnLaAl_{11}O_{19}$ (B), 0.33Pt-0.67Pd(0.27)/$MnLaAl_{11}O_{19}$ (C) and 0.67Pt-0.33Pd(1.1)/$MnLaAl_{11}O_{19}$ (D), calcined at 1000 °C.

catalyst based on Al_2O_3. The $PtPd/Al_2O_3$ catalysts did not change their activity in the oxidation of methane at 500 °C in the presence of up to 2.5 vol.% of water vapor, when their Pt/Pd atomic ratio was within the range of 0.5–1.0 [39]. On the other hand, these catalysts significantly decreased their activity at water content 5 vol.% and higher [39], however, they quickly regained their catalytic performance after removing water vapor from the reactant mixture. Note that Pd-based catalysts in our study as well as in other studies [39,45] restored only partially after removing water vapor from the reactant mixture, while the Pt-modified Pd-Mn-hexaaluminate catalysts with the atomic ratio of Pt/Pd < 0.27 regained their catalytic performance. So, the low Pt loading has the positive effect on the resistance of Pd-based catalysts to the deactivation with water vapor.

As compared with water vapor, sulfur dioxide has a higher deactivating effect on the efficiency of the oxidation of methane on Mn-hexaaluminate and on the monometallic Pd-Mn-hexaaluminate catalysts. The methane conversion in the presence of 1000 ppm SO_2 in the reactant mixture drops to 90% on both $MnLaAl_{11}O_{19}$ (Fig. 1A) and 0.82Pd(0)/$MnLaAl_{11}O_{19}$ (Fig. 1B). The similarity of their behaviors is likely due to Mn-sulfate originated from Mn-hexaaluminate in the presence of SO_2. The formation of manganese sulfate at 800 °C is well known for Mn_3O_4-containing catalysts [47]. The bimetallic catalyst in which 0.33 wt% of Pd are substituted with platinum (Pt/Pd = 0.27) showed the highest efficiency of the oxidation of methane (approximately 99%) within the dry methane-air mixture containing 1000 ppm SO_2 (Fig. 1C). It is probably because Pt inhibits adsorption of SO_2 on palladium particles [31] and catalyzes worse oxidation of SO_2 to SO_3 than PdO and Pd [23]; as a result, the formation of Mn-sulfate is suppressed.

The deactivating influence of sulfur dioxide was amplified with water added to the air-fuel feed. This effect had been described in detail for PdO/Al_2O_3 [23], but it was found that it is also typical of Mn-hexaaluminate and the monometallic Pd-catalysts based on $MnLaAl_{11}O_{19}$. For example, the methane conversion in their presence decreased from 99% to 85–87% and from 95% to 82–83% over Mn-hexaaluminate and the Pd-Mn-hexaaluminate catalysts, respectively (Fig. 1A and 1B). It was harder to predict the lower resistance of the bimetallic catalyst with a high Pt content to the deactivation with sulfur dioxide in the presence of water vapor. Thus, the bimetallic 0.67Pt-0.33Pd(1.1)/$MnLaAl_{11}O_{19}$ catalyst with Pt/Pd = 1.1 underwent the most significant deactivation in the presence of water vapor and SO_2 in the reactant mixture, the CH_4 conversion at 670 °C fell from 90% to 30% after adding water with sulfur dioxide (Fig. 1D). So, when water and sulfur dioxide are input in the methane-air feed, the Mn-hexaaluminate catalyst shows also the high activity in the methane oxidation comparable in some aspects to the catalyst 0.8Pd(0)/$MnLaAl_{11}O_{19}$ and superior to 0.67Pt-0.33Pd(1.1)/$MnLaAl_{11}O_{19}$. On the other hand, 0.33Pt-0.67Pd(0.27)/$MnLaAl_{11}O_{19}$ with a low content of Pt (0.33 wt% Pt, Pt/Pd = 0.27) kept its stability and maintained methane conversion close to 99% (Fig. 1C). Therefore, the catalyst stability depends greatly on the Pt/Pd atomic ratio, and thus on the state of the active component.

Literature data provide contradictory points of view on the mechanism of the deactivating influence of water vapor and sulfur dioxide on the efficiency of the oxidation of methane on

monometallic Pd-based catalysts and bimetallic PtPd-based catalysts. Some authors believe that the deactivation with water vapor and sulfur dioxide is of adsorption character, i.e. related to competitive adsorption. This assumption is based on the fact of the bimetallic catalyst quickly recovering its activity after the removal of water vapor from the reactant mixture [39], whereas the monometallic Pd-based catalysts regenerate only partially [39,45]. The adsorption character of the interaction of water and SO_2 with the catalyst surface is also indicated by the sharply rising resistance of the catalyst to the deactivation with water vapor [11,12,14,15] and sulfur dioxide [18,24] with temperature. According to another point of view, the hydroxylation of PdO surface with water [14,15,44] and the sulfation of PdO particles [18–20] and surface/volume of the support [18,21–23,47] with sulfur dioxide indicate the chemisorption character of the catalyst deactivation.

In our work we have tried to reveal the origin of the catalyst deactivation with water vapor and sulfur dioxide by comparing the temperature dependences of the oxidation of methane on the fresh and deactivated catalysts in the absence of the catalytic poisons. As the data given in Fig. 2 show, at 10,000 h^{-1} the temperature of reaching 50% of the methane conversion on all studied catalysts increases after testing them in the presence of water vapor and SO_2. The greatest shift of the temperature dependence of methane conversion (more than 200 °C) is observed for the deactivated 0.67%Pt-0.33%Pd(1.1)/$MaLaAl_{11}O_{19}$ catalyst with a high platinum loading (Fig. 2D), the highest methane conversion under the selected conditions reaching 35%. The lowest change in the temperature of 50% conversion (no more than 60 °C) was found for the 0.33Pt-0.67Pd(0.27)/$MnLaAl_{11}O_{19}$ catalyst (Fig. 2C), which is not subjected to the deactivation by water or/and sulfur dioxide at high temperatures near 670 °C (Fig. 1C). The shift of the temperature dependence of methane conversion for the deactivated catalyst to the high-temperature area indicates that the chemical composition of the catalyst surface does not return to the initial state after the removal of water and SO_2 from the reaction feed, which means that the reason for the deactivation is chemisorption of the catalytic poisons. The greater the shift of temperature of 50% of methane conversion to the high-temperature region, the higher the deactivating effect of water and SO_2 over the catalyst. We should note that the deactivated bimetallic 0.33Pt-0.67Pd(0.27)/$MnLaAl_{11}O_{19}$ catalyst converted methane more efficiently than the monometallic 0.82Pd(0)/$MnLaAl_{11}O_{19}$ catalyst, whereas the fresh bimetal catalyst was less active than the monometallic one. 50% conversion of methane on the deactivated catalysts was reached at temperatures of 430 and 545 °C, respectively. For the fresh catalysts the temperature of 50% methane conversion was 370 and 355 °C, respectively.

Table 1 presents the pre-exponential factor and the observed activation energy calculated from the experimental temperature dependences of methane oxidation over the fresh catalyst and the catalyst tested in the presence of water and SO_2 (Fig. 2). The comparison of the characteristics of the formal kinetics for the fresh and deactivated catalysts showed that both a decrease in the pre-exponential factor and a drop in the observed activation energy were registered for the deactivated catalysts. The only exclusion was the 0.33Pt-0.67Pd(0.27)/$MnLaAl_{11}O_{19}$ catalyst, for which the change in the activation energy was within the experimental error, and the pre-exponential factor decreased fourfold. A decrease in k_0 with close E_a indicates that the deactivated 0.33Pt-0.67Pd(0.27)/$MnLaAl_{11}O_{19}$ catalyst contains a smaller number of active centers than the fresh catalyst. For other catalysts the observed activation energy decreased from 72 ± 3 to 41–54 kJ/mol. However, the texture characteristics of the fresh and deactivated catalysts differ insignificantly (Table 1): the specific surface decreases by 25%, the pore volume reduces by no more than 8-10%, the prevailing pore radius does not change and is 22–25 nm. Considering the fact of the insignificant change in the texture characteristics the observed decrease in the activation energy cannot be explained by the influence of the diffusion restrictions over the formal kinetics of methane oxidation on the deactivated catalysts. The assumption remains that the state of the active component in the catalyst changes in the presence of water and SO_2.

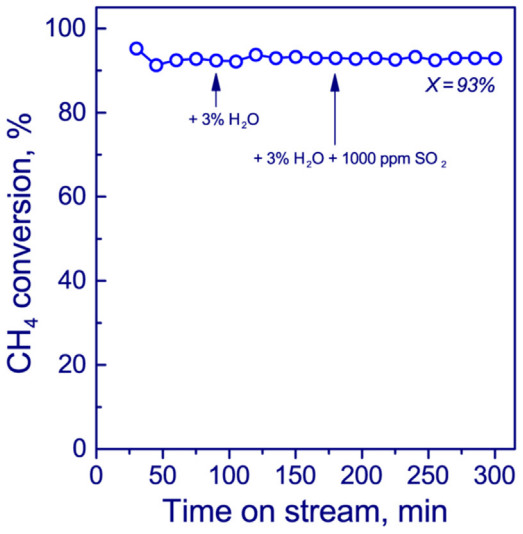

Fig. 3. Methane conversion on the 0.33Pt-0.67Pd(0.27)/$MnLaAl_{11}O_{19}$ catalyst at 495 °C in the presence of water vapor (3 wt%) and sulfur dioxide (1000 ppm).

Therefore, among the studied catalysts, the Pt-doped Pd-Mn-hexaaluminate catalyst with Pt/Pd = 0.27 was the most resistant to water and sulfur dioxide (Fig. 1C). Note that this catalyst was also resistant to the deactivation at a lower temperature (500 °C), when a high deactivation of PdO/Al_2O_3 is usually observed [32]. The 0.33Pt-0.67Pd(0.27)/$MnLaAl_{11}O_{19}$ catalyst provided for the methane conversion of 93% at 495 °C and 10,000 h^{-1} both in the dry methane-air mixture and in the presence of water and SO_2 (Fig. 3). Besides, the high catalytic activity of Mn-hexaaluminate is inhibited weakly by water and/or SO_2 compared with the Pd-based catalysts and the bimetallic high Pt-loaded Pt,Pd-catalyst.

The difference in the catalytic behavior of Pd-containing catalysts based on Al_2O_3 is usually linked to the different states of palladium in them. It is believed that PdO is subjected to the deactivation with water vapor [32], and metallic Pd or its alloys with Pt are resistant to the deactivation [33]. PdO sulfates in the presence of sulfur dioxide [48–51], as the particles of metallic Pt inhibit the adsorption of SO_2 on PdO [52]. Meanwhile, it is considered that a part of sulfur from PdO surface can diffuse to the surface of the sulfating supports [53] or be removed at temperatures exceeding 600 °C [48,54] causing a partial regeneration of the catalyst [54,55]. In order to reveal the reasons for the high efficiency of the oxidation of methane on the bimetallic PtPd-catalyst based on $MnLaAl_{11}O_{19}$ and its high resistance to the deactivation with water and sulfur dioxide we have studied the morphology of the noble metal particles, the state of Pt and Pd in the fresh and deactivated catalysts, their redox properties, and compared the obtained characteristics with the properties of the monometallic Pd-catalyst and the support based on Mn-hexaaluminate.

3.2. XRD-composition and particle morphology in Pt-Pd-modified Mn-hexaaluminate

The composition and particle morphology of active site in the Pd- and PtPd-modified Mn-hexaaluminate catalysts were studied by XRD and HRTEM. According to XRD (Table 1) and HRTEM data (Fig. 4 and 5) the Pd- and PtPd-modified Mn-hexaaluminate catalysts contain the crystallized phases of hex-

Table 1
Main physicochemical and catalytic characteristics of fresh and spent Pd- and PtPd-modified catalysts based on $MnLaAl_{11}O_{19}$; the testing in the methane oxidation was in the presence of water vapor and SO_2 (*deact*).

№	Active component composition	Chemical composition, wt%, and atomic ratio of Mn, La, Pt, Pt to Al					Phase composition	Texture characteristics		Temperature of x% CH_4 conversion[b]		Kinetic parameter of CH_4 oxidation at 10000 h^{-1}	
		Mn	La	Pd	Pt	S		S_{BET}, m^2/g	V_Σ, cm^3/g	$T_{50\%}$, °C	$T_{90\%}$, °C	E_a, kJ/mol	k_0, c^{-1}
1[a]	$MnLaAl_{11}O_{19}$	7.10 *0.083*	9.95 *0.047*	–	–	–	$MnLaAl_{11}O_{19}$ (S_{37} = 40)[c]; $LaAlO_3$ (S_{27} = 50); γ^*-Al_2O_3 (a = 7.936 Å)[d]	44	0.24	460	560	72 ± 3	3.1×10^5
2[a]	$MnLaAl_{11}O_{19}$-*deact*	7. 08	9.95	–	–	0.76	$MnLaAl_{11}O_{19}$ (S_{37} = 200); $LaAlO_3$ (S_{27} = 50)	36	0.21	585	680	41 ± 3	560
3	1.0Pd(0)	7.10 *0.083*	9.95 *0.047*	0.82 *0.005*	–	–	$MnLaAl_{11}O_{19}$ (S_{37} = 60); $LaAlO_3$ (S_{27} = 50); γ^*-Al_2O_3 (a = 7.936 Å); PdO (100–120 Å)[e]; Pd^0 (highly disp., trace)	48	0.24	460	575	110 ± 6	6.9×10^8
4	1.0Pd(0)-*deact*	7.20	9.89	0.81	–	0.87	$MnLaAl_{11}O_{19}$ (S_{37} = 230); $LaAlO_3$ (S_{27} = 60); γ^*-Al_2O_3 (a = 7.937 Å); PdO (400 Å, S_{39} = 160); Pd^0 (disp., S_{41} = 90)	36	0.22	545	680	72 ± 3	7.5×10^4
5	0.33Pt-0.67Pd (0.27)	7.10 *0.083*	9.95 *0.047*	0.67 *0.004*	0.33 *0.001*	–	$MnLaAl_{11}O_{19}$ (S_{37} = 60); $LaAlO_3$ (S_{27} = 50)	46	0.26	370	475	70 ± 2	8.5×10^5
6	0.33Pt-0.67Pd (0.27)-*deact*	7.05	9.84	0.69	0.30	0.30	$MnLaAl_{11}O_{19}$ (S_{37} = 250); $LaAlO_3$ (S_{27} = 50)	35	0.24	430	525	67 ± 7	2.1×10^5
7	0.67Pt-0.33Pd (1.1)	7.10 *0.083*	9.95 *0.047*	0.33 *0.002*	0.67 *0.002*	–	$MnLaAl_{11}O_{19}$ (S_{37} = 60); $LaAlO_3$ (S_{27} = 50)	50	0.25	455	590	57 ± 2	1.9×10^4
8	0.67Pt-0.33Pd (1.1)-*deact*	7.25	9.77	0.33	0.66	0.64	$MnLaAl_{11}O_{19}$ (S_{37} = 245); $LaAlO_3$ (S_{27} = 40)	38	0.24	[b]	[b]	41 ± 3	240

[a] – MnLaAl11O19 sample does not contain Pd and Pd.
[b] – 50% and 90% methane conversion is not reached under the chosen conditions.
[c] – intensity of the strongest line of this XRD-phase observed on a diffraction pattern is specified in brackets.
[d] – a solid solution based on γ-Al_2O_3 structure with indicated lattice parameter α.
[e] – dispersion of this phase is specified in brackets.

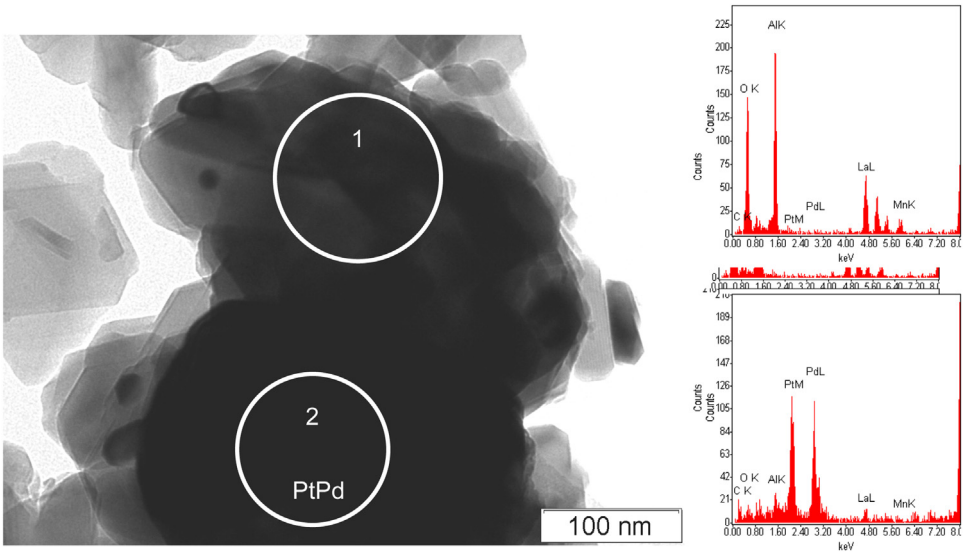

Fig. 4. Morphology of particles and corresponding EDX-spectra typical of PtPd-modified catalyst based on $MnLaAl_{11}O_{19}$. The catalyst is 0.33Pt-0.67Pd(0.27)/$MnLaAl_{11}O_{19}$.

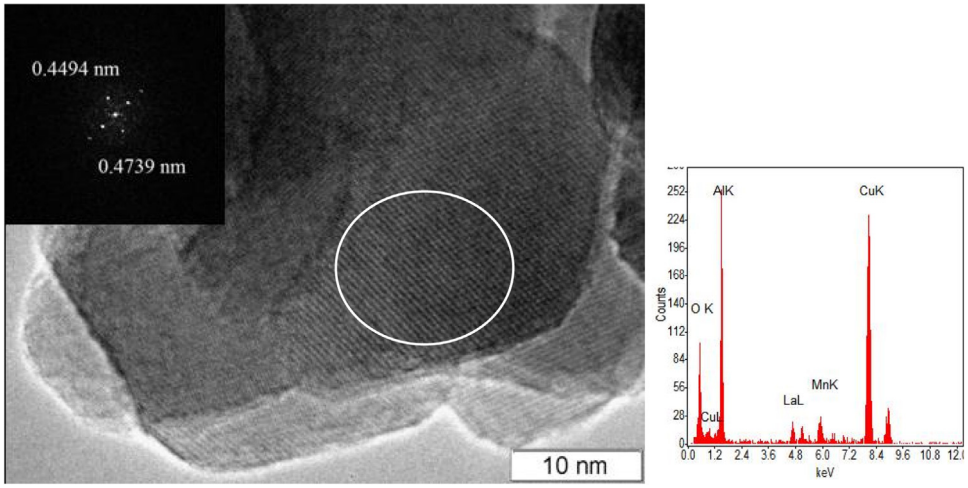

Fig. 5. HRTEM image of $MnLaAl_{11}O_{19}$ particle. Inserts in Figure show the EDX spectrum and FFT image obtained from the area of TEM image marked by a white circle.

aaluminate $MnLaAl_{11}O_{19}$ (36-1317) and perovskite $LaAlO_3$ (31-22). $MnLaAl_{11}O_{19}$ crystallites have a prismoidal shape in 150–200 nm in width and 400–600 nm in length (Fig. 4(1)). $LaAlO_3$ crystallites have primarily epitaxial binding with the $MnLaAl_{11}O_{19}$ crystallites [41,46]. The monometallic 0.82Pd(0)/$MnLaAl_{11}O_{19}$ catalyst contains PdO phase with coherent scattering region of 10–12 nm and the coarsely dispersed metal Pd phase. The XRD data are corroborated by the HRTEM results, according to which the interplanar distances in the highly dispersed particles of noble metal correspond to PdO (Fig. 6B). In addition to the highly dispersed PdO particles, the particles of metal Pd were registered with the size of 30 nm and more. The particles of metal Pd are covered with a layer of PdO 3–5 nm thick (Fig. 6A).

It is difficult to estimate the presence of crystallized phases of metal Pt and Pd in the bimetallic PtPd-catalysts using the XRD data, because the content of Pt and Pd is low and the basic reflexes of the indicated phases overlap those of $MnLaAl_{11}O_{19}$. According to the HRTEM data, the metal particles containing Pd and Pt have large sizes of 100–500 nm (Fig. 4(2)); however, PdO particles of 3–25 nm in size are also observed (Fig. 6B). We failed to fix the PdO film over the surface of the metal particles in the bimetallic catalysts. Therefore, we can suppose that the metal particles consist of PdPt alloy, which is not oxidized when contacting the atmospheric air unlike metal palladium. Besides, we previously registered very small Pt nanoparticles (3–5 nm) on HRTEM images of the Pt-doped Pd-Mn-hexaluminate catalysts prepared from chloride precursors and having the Pt/Pd atomic rato equal to 1.1 [46]. Though the particles of PtOx and Pt have not been recorded by HRTEM in the ex-nitrate bimetallic catalysts, we can not exclude their existence in the high Pt-loaded catalyst. This will be confirmed with the H_2-TPR data. No formation of Mn or Al sulfates as well as no changes in the phase composition and morphology of the noble metal particles has been detected with XRD and TEM in both mono- and bimetallic catalysts tested in the methane oxidation in the presence of water vapor and SO_2. However, with the help of local EDX analysis we have found sulfur unevenly distributed over the surface of the deactivated catalyst. Its content on the particles of Mn-hexaaluminate varied within a wide range, from 0.3 to 3.5 wt%. In the deactivated 0.82Pd(0)/$MnLaAl_{11}O_{19}$ monometallic catalyst the concentration of sulfur on/in the particles containing 35–40 wt% Pd was 0.2–0.8 wt%, and on/in the bulk particles of metal Pd (85–92 wt%) it did not exceed 0.33 wt%. In the deactivated 0.33Pt-0.67Pd(0.27)/$MnLaAl_{11}O_{19}$ and 0.67Pt-0.33Pd(1.1)/$MnLaAl_{11}O_{19}$ bimetallic catalysts sulfur was absent in

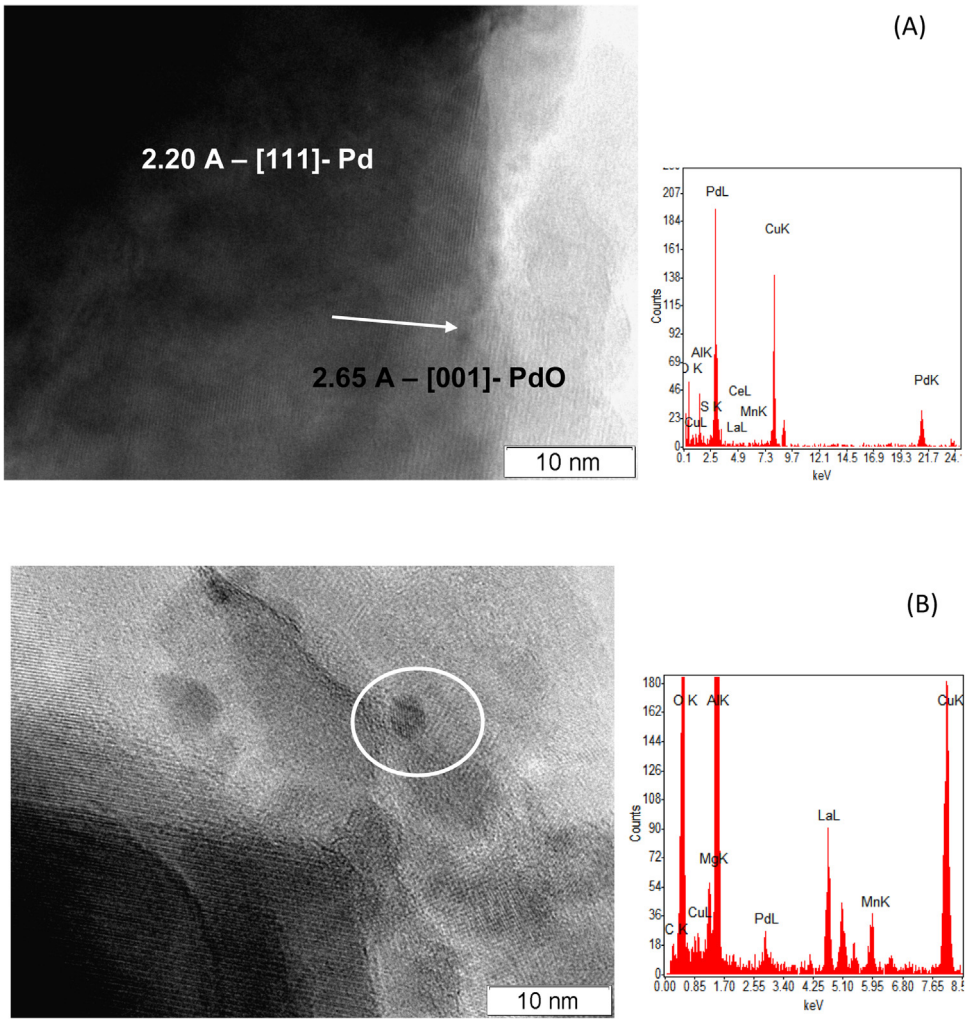

Fig. 6. HRTEM image of particle of metal palladium covered with PdO layer (A) and highly dispersed PdO (B) with corresponding interplanar distances and EDX-spectra.

the sites of localization of the large particles of the PtPd alloy (87–91 wt%), and its content in the areas of EDX analysis with the content of noble metals 25–45 wt% did not exceed 0.25 wt%. Therefore, we can use the EDX analysis data to conclude that sulfur has a tendency to localize on the particles of Mn-hexaaluminate, and not on the particles of noble metals. Our EDX data correlate with the revealed fact that PdO promotes the sulfation of sulfating supports (for example, Al_2O_3 and ZrO_2 [19]) due to conversion of SO_2 to SO_3 [20–23], at the same time the sulfation of PdO particles diminishes [18].

3.3. State of main components of fresh and spent Pt-Pd-modified Mn-hexaaluminate

The state of active component in the Pd- and PtPd-modified Mn-hexaaluminate catalysts was studied by XPS and DTA. The relative concentrations of the elements in the near-surface layer of the catalysts and the Al*2p*, Pt$4f_{7/2}$, Pd$3d_{5/2}$, O*1s*, Mn$2p_{3/2}$, and La$3d_{5/2}$ binding energies determined according to the XPS data are given in Tables 2 and 3, respectively.

The atomic ratios [Mn]/[Al] and [La]/[Al] in the near-surface layers in Mn-hexaaluminate as well as in the monometallic and bimetallic PtPd-catalysts were 0.07–0.08 and 0.04–0.10, respectively. These values are close to the bulk ratio of these components in the catalysts based on $MnLaAl_{11}O_{19}$ ([Mn]/[Al] = 0.083 and [La]/[Al] = 0.047) calculated by the AAS-ICP data (Table 1). Therefore, Mn and La are uniformly distributed in $MnLaAl_{11}O_{19}$. In some cases the observed ratios [La]/[Al] are lower than the stoichiometric ratio in $MnLaAl_{11}O_{19}$, which can be explained by the crystallization of a part of La within $LaAlO_3$. On the contrary, forming of the surface lanthanum carbonates results in an increase of the atomic ratio [La]/[Al]. The atomic ratio [O]/[Al] in the Pt,Pd-containing catalysts exceeds the stoichiometric value ([O]/[Al] = 1.70), which is explained by the presence of the near-surface carbonic oxygen-containing admixtures, in particular, lanthanum carbonates. The near-surface layer of Pd- and PtPd-modified catalysts is significantly enriched with Pd and Pt. The atomic ratios in the near-surface layers exceed the bulk ratios in the catalyst several times. The enrichment of the near-surface layers with a noble metal in case of its supporting from the solutions of Pd and Pt nitrates with a low concentration of free nitrate-ions ($[NO_3^-/Pd^{2+}] = 1$) is well known and described in literature [41,56]. The reason for the so-called egg-shell distribution of Pd and Pt is hydrolysis of their cations in the solutions.

For the deactivated catalysts, the atomic ratios [Mn]/[Al] and [La]/[Al] diminish, which indicates the enlargement of the $MnLaAl_{11}O_{19}$ crystallites during testing in the reaction medium. This assumption agrees well with the observed decrease in the specific surface area of the catalyst (from 40–45-to 35–38 m^2/g) as well as with an increase in the intensity of the reflexes of $MnLaAl_{11}O_{19}$ phase (Table 1). The atomic ratios [Pd]/[Al] and [Pt]/[Al] also

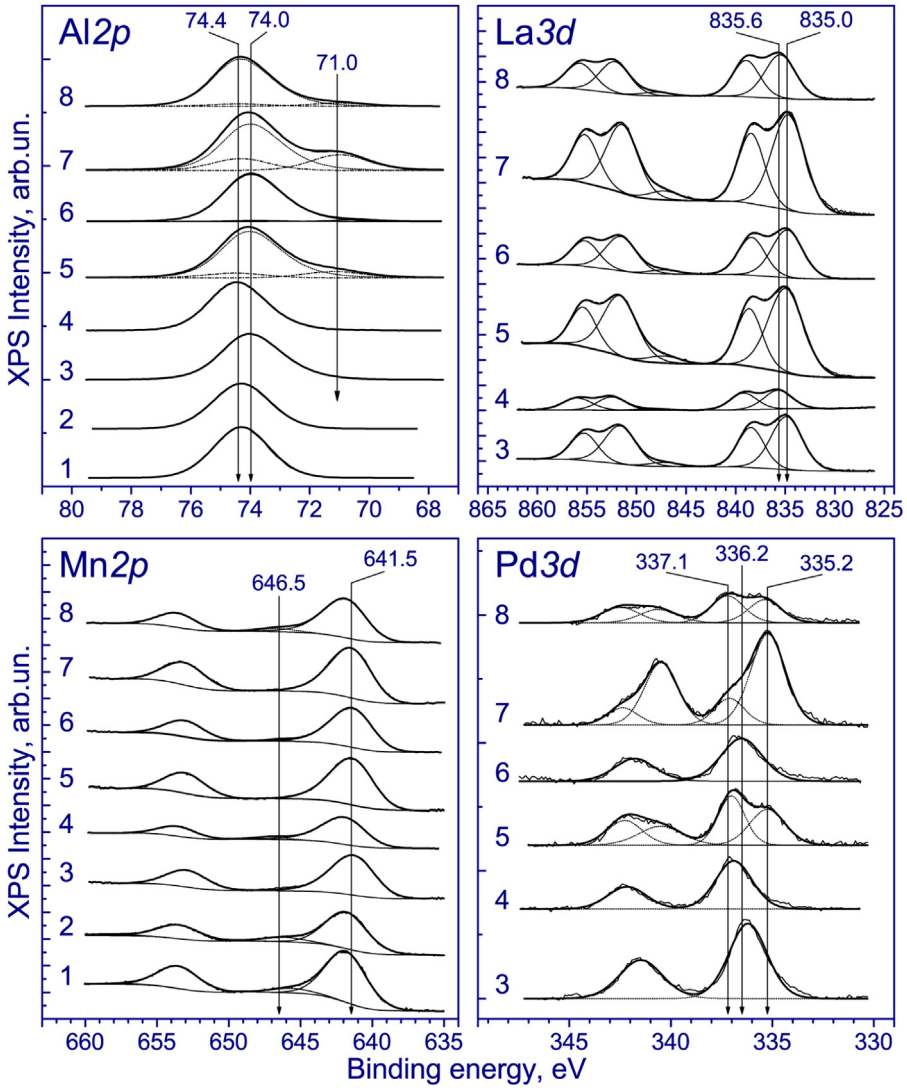

Fig. 7. Al*2p*, Pd*3d*, Mn*2p* and La*3d* spectra of the $MnLaAl_{11}O_{19}$ (*1,2*), 0.82Pd(0)/$MnLaAl_{11}O_{19}$ (*3,4*), 0.33Pt-0.67Pd(0.27)/$MnLaAl_{11}O_{19}$ (*5,6*) and 0.67Pt-0.33Pd(1.1)/$MnLaAl_{11}O_{19}$ (*7, 8*) catalysts, fresh (*1, 3, 5, 7*) and after testing in the methane oxidation in the presence of water vapor and SO_2 (*2, 4, 6, 8*). The Pt$4f_{7/2}$ – Pt$4f_{5/2}$ doublet is given in thin dashed line.

decrease in the deactivated catalysts, which signals the enlargement of the metal particles as a result of their sintering.

Fig. 7 presents the Al*2p*, Mn*2p*, La*3d*, and Pd*3d* spectra of the catalysts under study. The Al*2p* spectra of the fresh and deactivated $MnLaAl_{11}O_{19}$ catalysts as well as Pd- and PtPd-modified $MnLaAl_{11}O_{19}$ catalysts are described by a symmetric peak at 74.0-74.6 eV. The observed values of the Al*2p* binding energy are typical of Al^{3+} cations in the structure of alumina [48] and hexaaluminate [57,58].

The Mn*2p* spectrum is the Mn$2p_{2/3}$–Mn$2p_{1/2}$ spin-orbit doublet, with the integral peak intensities correlating as 2:1; the value of spin-orbit splitting is 11.8 eV. The asymmetric form of the peaks is determined by the many-electron processes. The Mn$2p_{3/2}$ binding energy for the mono- and bimetallic catalysts based on $MnLaAl_{11}O_{19}$ lies within the range of 641.1-641.7 eV (Table 3). The $MnLaAl_{11}O_{19}$ catalyst has a slightly larger value of the Mn$2p_{3/2}$ binding energy, 641.8 eV (Table 3). These values are close to the Mn$2p_{3/2}$ binding energy of the Mn^{3+} cations in Mn_2O_3 (641.5-641.9 eV [49–51]) and Mn^{2+} in MnO (640.4-641.7 eV [49–51,53]). To compare, MnO_2 is characterized by somewhat higher Mn$2p_{3/2}$ binding energies lying within the range of 642.2-642.6 eV [49,51]. In the Mn*2p* spectrum of $MnLaAl_{11}O_{19}$ catalyst we can also discriminate a weak shake-up satellite located at 3.7-4.4 eV above the value of binding energy with regard to the main Mn$2p_{3/2}$ peak. This shake-up satellite is typical of manganese in the Mn^{2+} state, its presence indicating that manganese in non-modified Mn-hexaaluminate is primarily in the Mn^{2+} state. The shake-up satellite is not manifested in the spectra of the fresh Pd- and PtPd-modified catalysts based on $MnLaAl_{11}O_{19}$, therefore modification of Mn-hexaaluminate by noble metals promotes oxidation of the manganese cations in the near-surface layer and their stability in the Mn^{3+} state. However, in the Mn*2p* spectra of the deactivated Pt,Pd-doped catalysts the shake-up satellite is clearly seen, which shows the prevalence of manganese in the Mn^{2+} state. Thus, we can suppose that the crystal structure of $MnLaAl_{11}O_{19}$ improves under the reaction conditions, which particularly agrees with the XDR data. At the same time, the stabilization of Mn^{2+} ions in the deactivated catalysts can be related to the formation of surface sulfates of Mn(II) in the presence of SO_2, observed with DTA and IR spectroscopy.

The La*3d* spectra are the La$3d_{5/2}$–La$3d_{3/2}$ spin-orbit doublet, each peak of which is accompanied with an intensive shake-up satellite. The intensive peaks of the shake up satellites are typical of La^{3+} compounds and are determined by the hybridization of O*2p*

and La*4f* orbitals [55]. The La$3d_{5/2}$ binding energy varies within a wide range from 834.8 to 835.7 eV (Table 3), which confirms the possibility of forming the surface carbonates and/or sulfates of lanthanum. The close values of the La$3d_{5/2}$ binding energy are observed for the double oxides (835.5-836.0 eV [57,58]), for example, lanthanum aluminate or Mn-hexaaluminate. For La_2O_3, the main La$3d_{5/2}$ peak lies within 833.2-834.0 eV [54,59,60]. For lanthanum carbonate $La_2(CO_3)_3$, somewhat higher values of the La$3d_{5/2}$ binding energy at 835.0-835.5 eV are observed [59,60]. The La$3d_{5/2}$ binding energy of LaOOH and $La(OH)_3$ hydroxides is in a close range, 834.8 eV [54,59].

As is known, the Pd*3d* spectrum is the Pd$3d_{5/2}$–Pd$3d_{3/2}$ spin-orbit doublet with the integral intensities of its components correlating as 3:2, and the value of spin-orbital splitting (difference between the Pd$3d_{5/2}$ and Pd$3d_{3/2}$ binding energies) is 5.26 eV. For palladium in the metal state, the Pd$3d_{5/2}$ binding energy is 335.0-335.2 eV [52,60], and for palladium oxide PdO, it is 336.6-337.7 eV [60,61,62]. The Pd*3d* spectra of the monometallic Pd-catalyst based on $MnLaAl_{11}O_{19}$ are well described by one Pd*3d* doublet with the Pd$3d_{5/2}$ binding energy 336.2 eV indicating the presence of PdO in the catalyst. The Pd$3d_{5/2}$ binding energy in the monometallic deactivated catalyst increases to 336.9 eV, but still corresponds to the Pd^{2+} state.

Spectra of the fresh bimetallic PtPd-catalysts based on $MnLaAl_{11}O_{19}$ are described by two Pd$3d_{5/2}$–Pd$3d_{3/2}$ doublets, the Pd$3d_{5/2}$ binding energies of which lie within the range of 335.2–335.4 and 337.0–337.2 eV and indicate the presence of the metal palladium and PdO (Table 3). However, after the reaction the Pd*3d* spectrum of PtPd-modified catalyst with the low ratio Pt/Pd = 0.27 is described by one doublet with the Pd$3d_{5/2}$ binding energy 336.2 eV, corresponding to Pd^{2+}. The spectra of deactivated catalysts with high concentration of Pt are still described by two doublets, although with somewhat higher values of the Pd$3d_{5/2}$ binding energy, 335.4 and 337.2 eV. Similar to the 0.33Pt-0.67Pd(0.27)/$MnLaAl_{11}O_{19}$ catalyst, an increase in the share of PdO is observed for the catalyst with high Pt content after the oxidation of methane.

The Al*2p* spectra of the bimetallic PtPd-modified catalysts before and after the reaction feature the additional lines related to the Pt$4f_{7/2}$–Pt$4f_{5/2}$ doublet of platinum. The value of spin-orbital splitting is 3.33 eV. The Pt$4f_{7/2}$ binding energy of PtPd-catalysts depends on the Pt/Pd ratio and decreases somewhat (71.2 and 71.0 eV) with the growth of Pt/Pd (from 0.27 to 1.1) in the fresh catalyst. In the deactivated catalysts we observed lower Pt$4f_{7/2}$ binding energy (70.5 and 71.0 eV). For the metal platinum the Pt$4f_{7/2}$ binding energies 71.1–71.2 eV are given elsewhere [63]. For PtO, PtO_2, and $Pt(OH)_4$ the Pt$4f_{7/2}$ binding energy are significantly higher, 72.25–72.4 eV [54,64], 74.0–74.1 eV [54,65], and 74.2–74.4 eV [54], respectively. Therefore, platinum is primarily in the metal state on the surface of PtPd-modified Mn-hexaaluminates both before and after methane oxidation. Besides, the XPS data do not provide a solid basis to judge about the formation of PtPd alloy, since the shifts of Pt$4f_{7/2}$ and Pd$3d_{5/2}$ peaks can be determined by the alloy formation as well as by the dispersion of the supported metal particles. For instance, the work [65] gives the Pt$4f_{7/2}$ and Pd$3d_{5/2}$ binding energies of 71.0 and 335.2 eV for the particles of PtPd alloy, which nearly coincides with the values observed for our 0.67Pt-0.33Pd(1.1)/$MnLaAl_{11}O_{19}$ catalyst, 71.0 and 335.3 eV.

XPS confirms the presence of sulfur on the surface of deactivated catalysts. The S*2p* spectra of these catalysts are described by one peak at approximately 168.7-169.1 eV (Fig. 8) corresponding to sulfur within SO_4^{2-} or SO_3^{2-} [66]. The lower values of the S*2p* binding energy of 161.1–161.7 eV are typical of sulfur within sulfides [67]. The XPS data on the sulfur state were confirmed with thermal analysis and IR spectroscopy.

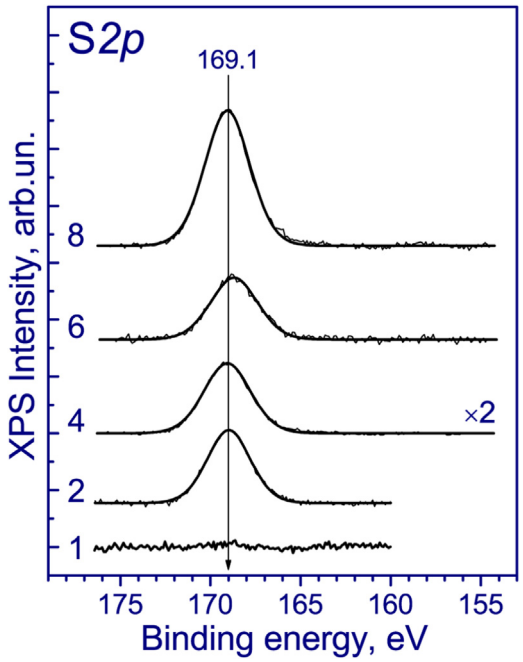

Fig. 8. S*2p* spectra of $MnLaAl_{11}O_{19}$ (*1*, *2*), 0.82Pd(0)/$MnLaAl_{11}O_{19}$ (*4*), 0.33Pt-0.67Pd(0.27)/$MnLaAl_{11}O_{19}$ (*6*) and 0.67Pt-0.33Pd(1.1)/$MnLaAl_{11}O_{19}$ (*8*) catalysts, fresh (*1*) and after testing in the methane oxidation in the presence of water vapor and SO_2 (*2*, *4*, *6*, *8*).

Fig. 9 presents the IR spectra of the Pd- and PtPd-modified catalysts tested in the oxidation of methane at 670 °C in the presence of water vapor and sulfur dioxide. All spectra feature a wide band at ~3400 cm^{-1} and a band at 1630 cm^{-1} related to the valence and deformation vibration of the adsorbed water, respectively [68]. In addition to these bands, the spectra also feature the band at 1145–1070 cm^{-1} corresponding to the asymmetric valence vibration of sulfate-ions with the tetrahedron-close symmetry [68]. The bands at 1000–250 cm^{-1} belong to the Metal-O vibrations.

The mass loss in the thermogravimetric analysis curves (Fig. 10) accompanied by an endothermic effect in the differential thermal analysis curves with the maximum in the temperature range of 104–114 °C is due to dehydration of the samples. The water content removed from the samples depended weakly on the catalyst composition and was about 1.1-1.6 wt%, with the indicated water amount being comparable with the amount of water removed in TG-DTA analysis of the fresh catalysts. A little mass loss with exoeffect was observed at 260 and 315–335 °C in the TG-DTA curves of both fresh and deactivated bimetallic catalysts and the Mn-hexaaluminate support. It is due to transformation of Mn^{3+}-containing phase. The next mass loss with the endothermic effect within the temperature range of 770–900 °C is likely to be related to the decomposition of sulfate-ions and their removal from the surface of the spent catalyst as SO_2. The assignment of these peaks to the decomposition of sulfate ions is consistent with the absence of the peaks in the region of 770–900 °C on the TG-DTA curves of the fresh Mn-hexaaluminate support. For the fresh catalysts 0.82Pd(0)/$MnLaAl_{11}O_{19}$ and 0.33Pt-0.67Pd(0.27)/$MnLaAl_{11}O_{19}$, containing particles of PdO, the mass loss in the temperature region 795–810 °C was also observed, but its value did not exceed 0.3 wt%. A minor weight loss by fresh samples at temperatures around 800 °C is caused by the decomposition of PdO to Pd. For the deactivated catalysts, the mass loss in 770–900 °C by the catalysts depended significantly on the catalysts composition and increased from 0.3 to 4.5 wt% in the following row: 0.33Pt-0.67Pd(0.27)/$MnLaAl_{11}O_{19}$ (0.3 wt%) < $MnLaAl_{11}O_{19}$ (2.7 wt%) < 0.82Pd(0)/$MnLaAl_{11}O_{19}$

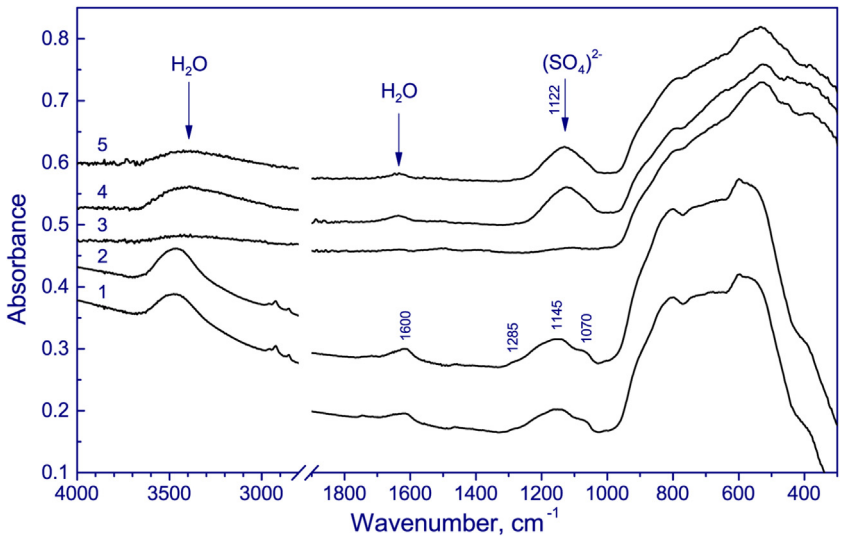

Fig. 9. IR-spectra of the $MnLaAl_{11}O_{19}$ (1), 0.82Pd(0)/$MnLaAl_{11}O_{19}$ (2), 0.33Pt-0.67Pd(0.27)/$MnLaAl_{11}O_{19}$ (3), 0.5Pt0.6-Pd(0.55)/$MnLaAl_{11}O_{19}$ (4), and 0.67Pt-0.33Pd(1.1)/$MnLaAl_{11}O_{19}$ (5) catalysts, tested in the methane oxidation in the presence of water vapor and sulfur dioxide.

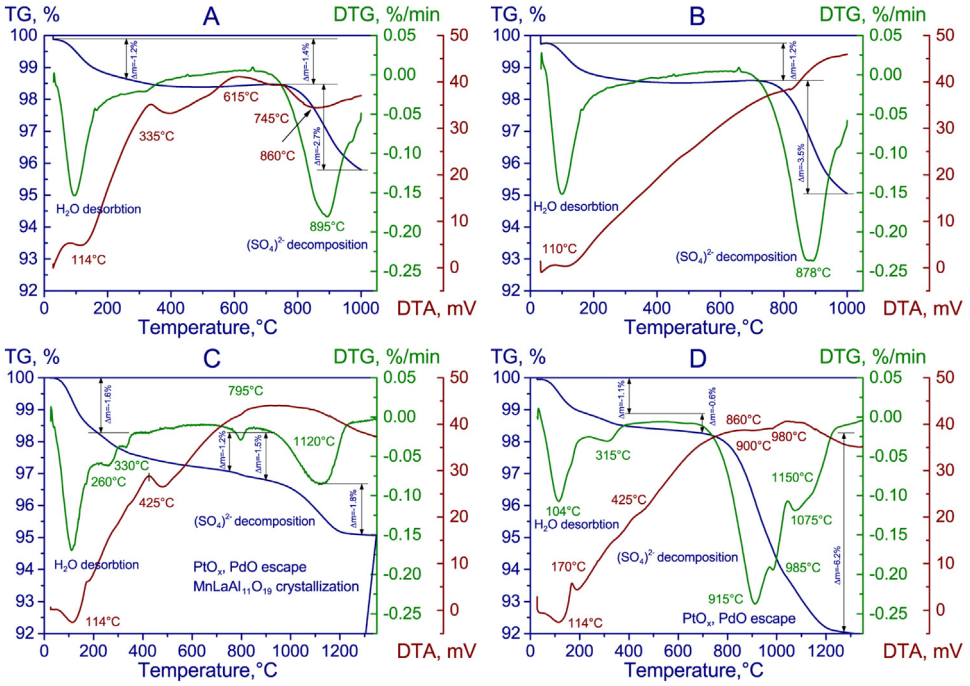

Fig. 10. TG-DTA curves of the $MnLaAl_{11}O_{19}$ (A), 0.82Pd(0)/$MnLaAl_{11}O_{19}$ (B), 0.33Pt-0.67Pd(0.27)/$MnLaAl_{11}O_{19}$ (C), and 0.67Pt-0.33Pd(1.1)/$MnLaAl_{11}O_{19}$ (D) catalysts, tested in the methane oxidation in the presence of water vapor and sulfur dioxide.

(3.5 wt%) < 0.67Pt-0.33Pd(1.1)/$MnLaAl_{11}O_{19}$ (4.5 wt%). On the one hand, this row correlates with the resistance of the catalysts to the deactivation with water vapor and SO_2, since 0.33Pt-0.67Pd(0.27)/$MnLaAl_{11}O_{19}$ is more resistant to the deactivation, and 0.67Pt-0.33Pd(1.1)/$MnLaAl_{11}O_{19}$ is more liable. According to the TG-DTA data for the Pt-Pd/$MnLaAl_{11}O_{19}$ catalysts, substitution of 0.33 wt% Pd by Pt resulted in a 11.6 times decrease in the mass loss in 800–900 °C, and, consequently, in SO_2 release. Thus, substitution of a small part of palladium with Pt actually helps to increase the sulfur-resistance of Pd-catalysts based on Mn-hexaaluminates. On the other hand, the mass loss by the catalyst 0.67Pt-0.33Pd(1.1)/$MnLaAl_{11}O_{19}$ in the region 770–915 °C is probably connected with the volatilization of the Pt-containing compounds, but not with decomposition of the sulfate ions. This assumption is discussed in detail below.

The temperature of decomposition of the surface sulfate-ions in the deactivated catalysts also depended on the catalyst composition. The highest temperature (about 895 °C) of the removal of sulfate-ions was typical of $MnLaAl_{11}O_{19}$. The sulfate-ion was removed from the surface of 0.82Pd(0)/$MnLaAl_{11}O_{19}$ monometallic catalysts at same temperatures (near 880 °C). When substituting a part of Pd with Pt a tendency has been observed for a decrease in the temperature of the removal of sulfate-ions, for example, with 0.33 wt% substitution of Pd with Pt the temperature of decomposition of sulfates drops to 795 °C, and with 0.67 wt% Pt, to 650–670 °C. The decrease in temperature of decomposition of surface sulfates observed in thermal analysis correlates with the resistance of bulk

sulfates of manganese, aluminum, palladium, and platinum to the thermal decomposition in oxidizing media, which decreases in the following row: Mn^{2+} (850 °C and higher) > Al^{3+} (820 °C) > Pd^{2+} (> 550 °C). Platinum sulfate hydrolyzes easily, and its formation in the reactant mixture containing water vapor and SO_2 is unlikely. Under air treatments, the sulfided Pd particles, which were formed at sulfidation of Pd/SiO_2 catalyst, transform to PdO at temperatures as low as 300 °C, while the sulfided Pt produce sulfate, PtO, and Pt in the metallic state at 500 °C [69]. Besides, in the oxidizing atmosphere, the decomposition temperature of aluminum sulfate was found to be significantly lowered (from 820 °C to 630 and 750 °C) in the presence of platinum [70]. Since the catalysts were tested at 670 °C, which is higher than the temperature of decomposition of bulk $PdSO_4$ (>550 °C) and supported $PdSO_4/PtSO_4$ (300 °C/500 °C), it is logical to presume the absence of the surface palladium and platinum sulfates in the deactivated catalysts; and all sulfur compounds located on $MnLaAl_{11}O_{19}$.

At a temperature above 900 °C for the bimetallic PtPd-catalysts based on $MnLaAl_{11}O_{19}$ we observed several intensive mass losses in the thermogravimetric analysis curves accompanied by weak exoeffects in the differential thermal analysis curves. These were peak at 1120 °C for 0.33Pt-0.67Pd(0.27)/$MnLaAl_{11}O_{19}$ and at 915, 985, 1075, and 1150 °C for 0.67Pt-0.33Pd(1.1)/$MnLaAl_{11}O_{19}$. TG-DTA analysis of the fresh bimetallic catalysts also displayed peaks at the same temperature range. Since these processes intensify and shift into the range of lower temperatures with an increase in the Pt content, it is possible to presume that they are due to evaporation of PtO_2 and PdO occurring intensively at a temperature above 900 °C [71].

Thus, the set of XRD, EDX, XPS, FTIR, and TG-DTA data indicates that sulfur indeed accumulates as sulfate-ions on the surface of the mono- and bimetallic PtPd-catalysts based on $MnLaAl_{11}O_{19}$ during the deactivation in the presence of water vapor and SO_2 in gas feed at 670 °C. According to the EDX and TG-DTA data, sulfate-ions are localized primarily over the surface of the crystallites of Mn-hexaaluminate phase and Al_2O_3, the latter being present in traces. We have not registered any proofs of the formation of $PdSO_4$ and $PtSO_4$. However, Mowery et al. [22,23] used infrared spectroscopy to demonstrate the formation of $PdSO_4$ in the supported PdO/Al_2O_3 and bulk PdO at a temperature of 500 °C, with the presence of water vapor in the reaction feed promoting its formation. The authors believed that the formation of $PdSO_4$ is determined by two factors. The first is oxidation of SO_2 to SO_3, which is catalyzed by PdO [23], and the second is adsorption of water vapor over the surface of Al_2O_3 that diminishes SO_2 adsorption due to the competitive sorption [23]. Using XPS, Wang et al. [69] suggested that Pd is converted mostly to PdO with some $PdSO_4$ by heating of Pd/SiO_2 at 500 °C in SO_2 (10 vol.%) and O_2 mixture, while Pt transforms largely to $PtSO_4$ under this condition. Note results obtained by Wang [69] are contrary to the thermodynamic data [72,73] and data of other authors [31,74–76]. Lambert et al. showed [74,75] that exposure of pre-oxidised Pt/Al_2O_3 catalysts to SO_2 results in preferential reaction of SO_2 with weakly bound oxygen at the Pt-O-Al interface, promoting interfacial sulfate formation and concomitant reduction of Pt. EXAFS, XPS and chemisorption measurements showed a formation of Pt-S bonds under sulfidation at reducing atmosphere and its complete reversal to Pt–O bonds when the Pt/SBA-15 catalysts had been exposed to typical NO oxidation conditions (300 °C, 300 ppm NO, 10–vol.% O_2) [76].

3.4. Redox properties of Pt-Pd-modified Mn-hexaaluminate

Fig. 11 presents the curves of temperature-programmed reduction by hydrogen of the mono- and bimetallic PtPd-catalysts based on $MnLaAl_{11}O_{19}$. In the H_2-TPR experiment unmodified Mn-hexaaluminate is characterized by the hydrogen consumption

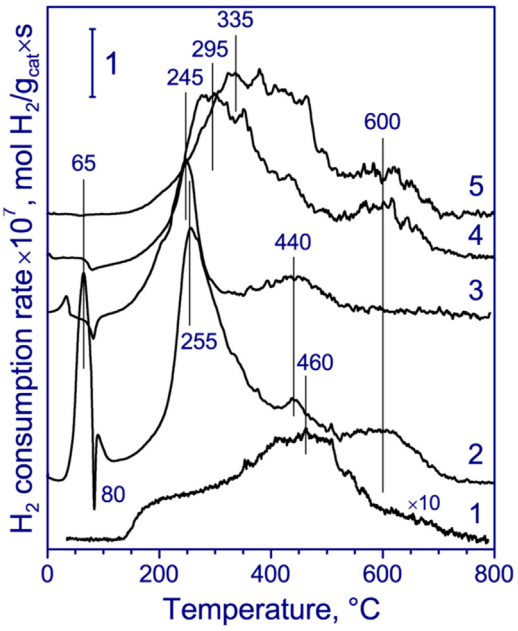

Fig. 11. H_2-TPR curves of the fresh PtPd/$MnLaAl_{11}O_{19}$ catalysts with the total content of noble metals of 1 wt% and various Pt/Pd atomic ratios, calcined at 1000 °C. $MnLaAl_{11}O_{19}$ (1), 0.82Pd(0)/$MnLaAl_{11}O_{19}$ (2), 0.33Pt-0.67Pd(0.27)/$MnLaAl_{11}O_{19}$ (3), 0.5Pt-0.6Pd(0.55)/$MnLaAl_{11}O_{19}$ (4), 0.67Pt-0.33Pd(1.1)/$MnLaAl_{11}O_{19}$ (5).

within a wide range of temperatures, 200–700 °C (Fig. 11, curve 1), which indicates the presence of Mn^{3+} cations and agrees with the XPS data on the state of manganese cations in the catalyst. We should note that the Mn^{3+} cations in $MnLaAl_{11}O_{19}$ were reduced within the same temperature range in which the bulk (330 and 460 °C [77]) and supported (400 and 485 °C [40]) Mn_2O_3 oxides are reduced, but without the clear manifestation of the stages of reduction, Mn_2O_3–Mn_3O_4–MnO, typical of Mn_2O_3. This is likely to be related to the localization of Mn^{3+} cations in the spinel blocks of hexaaluminates. The ratio of the amount of the consumed hydrogen to the manganese content in the catalyst (H_2/Mn) was 0.3, indicating the content of about 50% of manganese cations in the Mn^{3+} state.

The monometallic Pd-containing 0.82Pd(0)/$MnLaAl_{11}O_{19}$ catalyst intensively consumes hydrogen during the H_2-TPR experiment within the temperature ranges of 40–100 and 200–350 °C (Fig. 11, curve 2). The mentioned temperature ranges are usual for the reduction of the highly dispersed particles of PdO [78,79] and PdO particles with a strong interaction with the support [7,8,79], respectively. Reducing within the H_2-TPR experiment, the high-dispersed PdO firstly forms metal palladium and then palladium hydride. Pd hydride decomposes at 80 °C, which is indicated by the hydrogen release on the H_2-TPR curve [8,25,79]. Earlier we supposed that in the 1Pd(0)/$MnLaAl_{11}O_{19}$ catalyst calcined at 1200 °C the high-dispersed PdO is a thin layer covering the surface of the particles of metal palladium [79]. This assumption is confirmed here by the HRTEM data registered PdO layer over the surface of the metal Pd particles in the catalysts calcined at 1000 °C (Fig. 6A). This idea on the origin of the easily reducible Pd particles agrees well with the results of the works dedicated to the study of the catalytically active states of palladium. Thus, Burch et al. [11,26,80] showed the fast oxidation of metal Pd for the depth of several monolayers. McCarty [81] found that the hysteresis during methane burning is due to a layer of chemisorbed oxygen over the surface of palladium particle.

The H_2-TPR curves of the bimetallic PtPd-catalysts based on $MnLaAl_{11}O_{19}$ with the atomic ratio Pt/Pd within 0.05-0.3 are also characterized by a peak of desorption of hydrogen at 85 °C. However, the intensity of this peak is significantly lower than in

the H_2-TPR experiments with the monometallic Pd-catalyst. The amount of hydrogen released during the decomposition of palladium hydride depends on the Pt/Pd ratio in the bimetallic catalyst. It decreases as the Pt/Pd ratio grows from 0 to 0.55 (Fig. 11, curves 3, 4), and hydrogen desorption is absent when the ratio further increases up to 1.1 (Fig. 11, curve 5). According to the data by Bonarowska et al. [24,29], the absence of a peak of hydrogen desorption in H_2-TPR of Pd-containing catalysts is an indicator of formation of PdPt alloy, since the latter is not able to form palladium hydride.

The bimetallic PtPd-catalysts also contain the oxide compounds of Pd and Pt, reducing within the temperature range of 230–430 °C. PdO and PtO_2 with a strong interaction with the support are usually reduced within these temperature ranges [7,8,79]. As opposed to the monometallic Pd-catalyst, the amount of hydrogen consumed in this range decreases for the catalysts with the Pt/Pd ratio of 0.05–0.55, which may indicate a decrease in a PdO share. For the catalyst with Pt/Pd = 1.1, the amount of the consumed hydrogen grows, and the maximum of its consumption shifts to the area of high temperatures (430 °C). Comparing the literature data on the reduction of PtO_x and PdO [82–84], we can conclude that PtO_x reduces worse than PdO. Therefore, the described characteristics of the H_2-TPR curve confirms the presence of platinum oxide in the 0.67Pt-0.33Pd(1.1)/$MnLaAl_{11}O_{19}$ catalyst. In addition to that, the monometallic 0.82Pd(0)/$MnLaAl_{11}O_{19}$ catalyst and the bimetallic Pt-Pd(*w*)/$MnLaAl_{11}O_{19}$ catalysts are characterized by the hydrogen consumption with the maximum at 450-700 and 590 °C, respectively, resulting from the reduction of Mn^{3+} to Mn^{2+} [40,79]. Note that the amount of hydrogen consumed within this temperature range was significantly higher than it was observed for unmodified Mn-hexaaluminate. We can presume that a part of the cations of noble metal is incorporated into the structure of Mn-hexaaluminate and is reduced during the H_2-TPR within the temperature range of 450–700 °C along with the Mn^{3+} cations. Another reason for an increase in the hydrogen consumption in this area can be a growth of a share of the Mn^{3+} cations in the bimetallic catalyst as compared with Mn-hexaaluminate; the latter is due to particulate formation of Mn-nitrate from the Mn-hexaaluminate precursor during the supporting of Pt,Pd. Mn-nitrate transforms to Mn(III) ions at following calcination.

Thus, we can conclude that the bimetallic PtPd-catalysts based on $MnLaAl_{11}O_{19}$ with the Pt/Pd atomic ratio of 0.27 and lower contain several states of noble metal determining the redox potential of the catalytic system, such as, 1) particles of metal palladium or its alloy with Pt, 2) Pd or Pt oxide with a strong interaction with the surface of crystallites of Mn-hexaaluminate, and 3) Pt and/or Pd cations in the $MnLaAl_{11}O_{19}$ structure. In addition to that, the catalysts contain Mn^{3+} cations within Mn-hexaaluminate, which also influence the oxidizing ability of the catalyst. The share of each of the above listed states is determined by the Pt/Pd atomic ratio.

The redox properties of the bimetallic catalysts grow worse as the Pt/Pd atomic ratio increases to 0.27 and higher, primarily due to a decrease in the share of non-crystalline and highly dispersed PdO particles forming a layer over the surface of the metal Pd particles. An increase in the platinum share results in a drop in the amount of PdO in the catalyst due to the formation of PtPd alloy. The PtPd alloy implicitly influences the redox and catalytic properties of the bimetallic catalysts. This occurs due to the fact that the surface of the metal Pd particles reoxidizes easily with oxygen at a depth of several monolayers [11,26,78,80,81] forming non-crystalline or highly dispersed PdO, whereas the PtPd alloy does not have the ability to reoxidize the surface layer by oxygen even at a temperature of 500 °C and higher [35], used for catalyst pretreatment before the H_2-TPR experiment and for testing in the catalytic experiments. When the platinum content is increased, the redox properties of the bimetallic catalysts also worsen due to an increase in the share of PtO_2 particles with a strong interaction with the support. They reduce at higher temperatures (230–450 °C) [82–84] compared with the highly dispersed PdO, and metal Pt reoxidize not as easily [84,85] as Pd.

The ability of the mono- and bimetallic catalysts for the reduction with hydrogen changes after their testing at 670 °C in the methane oxidation in the presence of water vapor and SO_2 in the reactant mixture (Fig. 12). One can see a number of peculiarities in the H_2-TPR curve of the deactivated catalysts, the main of which is the appearance of a new wide peak at the temperature of 500–600 °C. This peak is characterized by a high intensity and is accompanied with hydrogen sulfide disengagement. The H_2S was identified by the photometric method with N,N-dimethyl-*p*-phenylendiamine after passing the stream from the TPR experiments through a solution of sodium hydroxide. Therefore, peak at 500–600 °C should be attributed to the reduction of the surface sulfate groups to hydrogen sulfide. The location of the peak's maximum as well as its intensity depended significantly on the catalyst composition, namely, on the Pt/Pd atomic ratio. Modifying of Mn-hexaaluminate by additions of Pd and Pt improved the process of sulfate groups reducing to H_2S and, consequently, their removal from the catalyst surface. The high temperature peak in the H_2-TPR curve shifted from 600 °C to 560 °C for the monometallic 0.82Pd(0)/$MnLaAl_{11}O_{19}$ catalyst and to 540 °C for the high Pt-loaded bimetallic PtPd-catalysts, indicating that Pt and PtPd alloy are stronger than Pd in terms of promoting the sulfates removal from the surface in the reduction conditions. Peak of H_2 consumption near 560 °C observed by us for the reduction of surface sulfate groups conforms to the H_2-TPR result for the sulfur-poisoned Pd/Al_2O_3 catalyst [19,86]. Yu and Shaw [19] showed that it corresponded to reduction of aluminum sulfate, resulting in Al_2O_3, SO_2, and H_2O. The second point is that a peak disappears completely in the area of 230–430 °C (Fig. 12, curves 2, 3, 5) in the H_2-TPR curves of the deactivated monometallic 0.82Pd(0)/$MnLaAl_{11}O_{19}$ catalyst and the bimetallic 0.33Pt-0.67Pd(0.27)/$MnLaAl_{11}O_{19}$ and 0.67Pt-0.33Pd(1.1)/$MnLaAl_{11}O_{19}$ catalysts. This peak corresponds to the reduction of highly dispersed oxide particles of PdO and PtO_x characterized by a strong interaction with the support. The third characteristic is that the decrease of the intensity of the low-temperature peak indicates a change in the share of easily reduced non-crystalline and highly dispersed PdO particles and metal Pd. For example, in the H_2-TPR curves of the deactivated 0.82Pd(0)/$MnLaAl_{11}O_{19}$ catalyst (Fig. 12, curve 2), the particles of highly dispersed PdO with a weak interaction with the support are characterized by a narrow peak at 50 °C as opposed to the fresh catalyst reducing within a wider range of temperatures (40–95 °C, Fig. 11, curve 2). This can be linked to the size homogeneity of the highly dispersed PdO particles in the deactivated catalyst, which is possible in the case of their location as oxide layer covering the surface of metal Pd particles. The share of metal Pd in the deactivated monometallic 0.82Pd(0)/$MnLaAl_{11}O_{19}$ catalyst increases, and its particles enlarge. Sintering of Pd^0 particles is indicated by a decrease in the peak intensity of hydrogen release at 85 °C in the H_2-TPR curve of the deactivated catalyst (Fig. 12, curve 2) as compared with the spectrum of the fresh catalyst (Fig. 11, curve 2).

The changes in the H_2-TPR curve of the bimetallic 0.33Pt-0.67Pd(0.27)/$MnLaAl_{11}O_{19}$ catalyst, namely, the decrease in the intensity of consumption and release of hydrogen at the temperature of 45–90 and 85 °C, respectively (Fig. 12, curve 3), reveal a decrease in the share of highly dispersed PdO particles with a weak interaction with the support and the share of metal particles, probably at the expense of an increase in the share of the PtPd alloy. A growth of Pt content in the 0.67Pt-0.33Pd(1.1)/$MnLaAl_{11}O_{19}$ catalyst leads to a complete disappearance of Pd^0 particles, and, consequently, non-crystalline PdO particles within the oxide film, as a result of which the deactivated catalyst contains only the PtPd

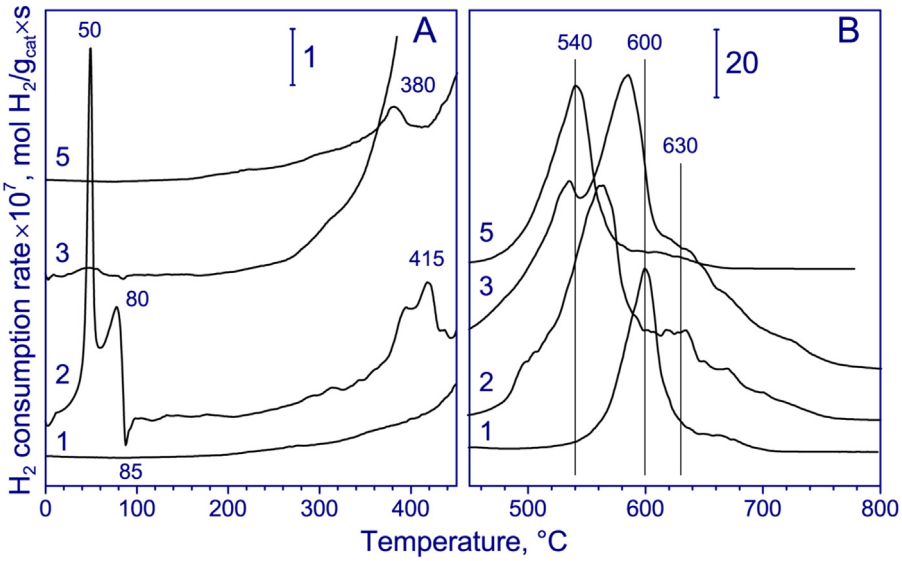

Fig. 12. H_2-TPR curves (A, low-temperature area, B, high-temperature area) of deactivated PtPd/$MnLaAl_{11}O_{19}$ catalysts with the total content of noble metals of 1 wt% and various Pt/Pd atomic ratios, calcined at 1000°C. $MnLaAl_{11}O_{19}$ (1), 0.82Pd(0)/$MnLaAl_{11}O_{19}$ (2), 0.33Pt-0.67Pd(0.27)/$MnLaAl_{11}O_{19}$ (3), 0.67Pt-0.33Pd(1.1)/$MnLaAl_{11}O_{19}$ (5).

alloy and is characterized by an absence of the peaks in the low-temperature area of the TPR-H_2 curves (Fig. 12, curve 5).

The declining of the catalytic activity of the PtPd-catalysts based on $MnLaAl_{11}O_{19}$ after their deactivation in the presence of water vapor and SO_2 can be explained by the observed changes in the composition of active particles in the deactivated mono- and bimetallic catalysts determining the redox properties of the catalysts, such as a decrease in the share of non-crystalline and highly dispersed PdO particles covering the surface of the metal Pd particles, an enlargement of Pd^0 particles or an increase in the share of the PtPd alloy, as well as the absence of the highly dispersed PdO and PtO_x particles with a strong interaction with the support.

3.5. Comparison of structure of active site in fresh and spent PtPd-modified Mn-hexaaluminate with their methane oxidation performance

Physical adsorption of water over the catalyst surface and chemisorption of OH-groups and sulfate-ion over the surface of the support and/or active component could be considered as a reason for the deactivation of PtPd-modified $MnLaAl_{11}O_{19}$. To reveal the possible reasons, the spent catalysts were studied with a complex of physicochemical methods. According to XRD and XPS, the decrease in the specific surface area of the catalysts based on Mn-hexaaluminate (from 43–45 m^2/g to 37 m^2/g) is likely to be due to the crystallization of $MnLaAl_{11}O_{19}$ and agglomeration of its particles under a high temperature and water presence, however, this decrease was not significant enough to be linked to the observed effects of deactivation of the mono- and bimetallic PtPd-based catalysts in the presence of water and sulfur dioxide.

XRD and HRTEM indicated that structure of the aluminate phase in the spent catalysts is not changed, interplanar distances characteristic for $MnLaAl_{11}O_{19}$ remain the same. The EDX data showed there is sulfur which mainly settles down on large particles of the Mn-hexaaluminate phase, while the sulfur is not present on the Pd and PtPd particles. The FTIR absorption band at 1145–1065 cm^{-1} and the S2*p* binding energy near 168.7–169.1 eV confirmed sorption of sulfur as sulfate-groups on the surface of the Mn-hexaaluminate crystallites. The sulfate content in them and temperature of its decomposition, which were registered by X-ray fluorescence analysis (Table 1) and thermogravimetric DTA, depended on the catalyst composition and increased as PtPd(0.27)/$MnLaAl_{11}O_{19}$ < PtPd(1.1)/$MnLaAl_{11}O_{19}$ < $MnLaAl_{11}O_{19}$ < Pd/$MnLaAl_{11}O_{19}$. The FTIR and TG-DTA results correlate with the H_2-TPR data of spent catalysts.

The atomic ratio of the consumed hydrogen to the total content of noble metals in the 0.33Pt-0.67Pd(0.27)/$MnLaAl_{11}O_{19}$ catalyst calcined at 1000°C is approximately 0.80. This indicates that a larger part of noble metals, no less than 80%, is in the state close to PdO and PtO oxides. According to XPS results, no less than 50% of the surface palladium is the oxidized state. The oxides of noble metal in the 0.33Pt-0.67Pd(0.27)/$MnLaAl_{11}O_{19}$ catalyst reduce at a temperature close to that of reduction of the monometallic 0.82Pd(0)/$MnLaAl_{11}O_{19}$ catalyst, which explains the slight difference in the catalytic behavior of the mentioned catalysts in the oxidation of methane in the absence of catalytic poisons. As the highly dispersed PdO was the active species of 0.82Pd(0)/$MnLaAl_{11}O_{19}$ catalyst, so they also ensured oxidation activity of the bimetallic 0.33Pt-0.67Pd(0.27)/$MnLaAl_{11}O_{19}$ catalyst. Since there is no highly dispersed PdO in the Pt-highly-loaded bimetallic catalyst, for example 0.67Pt-0.33Pd(1.1)/$MnLaAl_{11}O_{19}$, and the main states are the PtPd alloy and PtO_x, both fresh and deactivated catalysts have the lowest activity among the studied catalysts. The observed regularity of the change in the redox and catalytic properties of Pd-catalysts after substituting a part of Pd for Pt correlates well with the known fact of a higher activity of bulk PdO and highly dispersed PdO covering the surface of Pd^0 as compared with the metal palladium as well as metal platinum and PtO_x. For example, Burch et al. [11,80] and Farrauto et al. [85] showed that bulk PdO [11,80,87] and Pd oxidized to the depth of more than 3–4 monolayers [11] are the most active. Bell et al. [79,88] demonstrated that the completely reduced palladium has a low activity at 280°C, but the activity increases as 6–7 monolayers of PdO form over the Pd particles. The Pd-based catalysts containing PdO as active species exhibit a superior catalytic activity in the oxidation of methane compared to Pt-based catalysts [1–3,89] and a large metal Pt crystallites are their active particles [75,90–92], while PtO_x is inactive to the hydrocarbon oxidation [31,75,76,92].

Having analyzed the results of the kinetic studies of methane oxidation on the fresh and deactivated catalysts, we assume that the deactivation of the catalysts is due to a decrease in the amount of catalytically active sites in the bimetallic 0.33Pt-0.67Pd(0.27)/$MnLaAl_{11}O_{19}$ catalyst and to a change in the state of active component in the other catalysts. Comparing the H_2-TPR

Table 2
Atomic ratios of elements in the near-surface layer of the fresh and spent Pd- and PtPd-modified catalysts based on $MnLaAl_{11}O_{19}$. The catalytic testing in the methane oxidation was performed in the presence of water vapor and SO_2 (*deact*).

No.	Active component composition	[Mn]/[Al]	[La]/[Al]	[Pd]/[Al]	[Pt]/[Al]	[O]/[Al]	[S]/[Al]
1	$MnLaAl_{11}O_{19}$	0.08	0.04	–	–	1.7	–
2	$MnLaAl_{11}O_{19}$-*deact*	0.06	0.03	–	–	1.7	0.05
3	0.82Pd(0)	0.07	0.05	0.007	–	1.8	–
4	0.82Pd(0)-*deact*	0.04	0.02	0.004	–	1.6	0.05
5	0.33Pt-0.67Pd (0.27)	0.08	0.09	0.007	0.009	2.0	–
6	0.33Pt-0.67Pd (0.27)-*deact*	0.06	0.05	0.005	0.002	1.7	0.02
7	0.67Pt-0.33Pd (1.1)	0.08	0.10	0.010	0.010	1.9	–
8	0.67Pt-0.33Pd (1.1)-*deact*	0.07	0.04	0.004	0.004	1.8	0.09

Table 3
The binding energies (eV) of the fresh and spent Pd- and PtPd-modified catalysts based on $MnLaAl_{11}O_{19}$.

No.	Active component composition	Al*2p*	Mn$2p_{3/2}$	La$3d_{5/2}$	Pd$3d_{5/2}$ (%)	Pt$4f_{7/2}$	O*1s*	S*2p*
1	$MnLaAl_{11}O_{19}$	74.3	641.8	834.8	–	–	531.1	–
2	$MnLaAl_{11}O_{19}$-*deact*	74.3	641.8	835.2	–	–	531.2	169.0
3	0.82Pd(0)	74.0	641.4	834.9	336.2	–	530.7	–
4	0.82Pd(0)-*deact*	74.6	641.7	835.7	336.9	–	531.3	169.1
5	0.33Pt-0.67Pd (0.27)	74.1	641.4	834.9	335.3 (50)337.0 (50)	71.2	530.8	–
6	0.33Pt-0.67Pd (0.27)-*deact*	74.1	641.1	834.8	336.2 (100)	70.5	530.7	168.7
7	0.67Pt-0.33Pd (1.1)	74.0	641.5	834.7	335.2 (80)337.1 (20)	71.0	530.7	–
8	0.67Pt-0.33Pd (1.1)-*deact*	74.4	641.6	835.5	335.4 (45)337.2 (55)	71.0	531.2	169.1

data for the fresh and deactivated catalysts we can conclude that a decrease in the number of non-crystalline and highly dispersed PdO particles affects the oxidation ability of the catalysts resulting in its diminution. The decrease in the number of non-crystalline and highly dispersed PdO particles can be a result of the enlargement of Pd particles, leading to a diminishing of the surface available for oxidizing at a depth of several monolayers. Sintering of the metal Pd particles, which was observed by XPS as a decreasing of the surface atomic Pd/Al ratio (Table 3), can be caused by water vapor at elevated temperatures.

The Pd-modified $MnLaAl_{11}O_{19}$ sample possesses the higher SO_2-resistance compared with Pd/Al_2O_3. Surface of both alumina [18,21,89] and our Mn-hexaaluminate catalysts are subjected to sulfating, because PdO catalyzes the oxidation of SO_2 to SO_3 [20–23]; and the latter migrates to the support [19,22]. However, $PdSO_4$ is suggested to form also on Pd/Al_2O_3 under the SO_2 exposure at 500 °C [18,21] and decompose in O_2 at temperatures above 600–650 °C [21,89]. The absence of $PdSO_4$ in the catalysts based on $MnLaAl_{11}O_{19}$ can be explained by a high stability of the high-temperature structure of hexaaluminate and its low specific surface area as compared with the low-temperature modifications of Al_2O_3 [22,23]. As a result, water adsorbs weakly over the surface of Mn-hexaaluminate and does not hydroxylate the surface creating a low competition for SO_2 adsorption and preventing PdO sulfatation.

The particles of PtPd alloy have a positive effect over the water and sulfur resistance of the bimetallic 0.33Pt-0.67Pd(0.27)/$MnLaAl_{11}O_{19}$ catalyst compared with the monometallic Pd-based catalyst. Similar to the metal platinum [23,71,73], the PtPd alloy does not have to be able to adsorb SO_2 and form the stable sulfates, since the surface of PtPd alloy does not oxidize in the oxidizing conditions. Literature presents no proof of the formation of $PtSO_4$ in the oxidizing conditions of oxidation of hydrocarbons, even in the presence of significant amounts of SO_2, except Wang's data [69]. This can be related to that, unlike for $PdSO_4$, the region of thermodynamic resistance of $PtSO_4$ lies beyond the limits of the normal pressure and temperatures used in the oxidation of hydrocarbons. Having calculated the thermodynamic potentials, the authors show [72] that the oxidized state of Pt and Pd is possible to be sulfate only. Since the Pd(111) plane, the most represented over the surface of the palladium particles, has a high affinity for the formation of the surface PdO species, Pd-based catalysts are characterized by the strong fixation with SO_3 [72] and the high deactivation by sulfur [22,23,25,26]. At the same time, the tendency to form the surface oxide on Pt(111) and, consequently, to fix SO_3 is much weaker for Pt-based catalysts [72]. Density functional study of SO_2 adsorption over Pt(111) showed that within the temperature range of 25–75 °C the adsorbed SO_x desorbs from it without being decomposed [73]. A part of adsorbed SO_x transforms to the sulfate groups, which, however, stay stable over the surface up to the temperatures lower than 175 °C [73]. These temperatures are much lower than operating temperatures for the catalytic combustion chambers of the low-power gas plants. So, the distinction of particles of Pd, Pt, and PtPd alloy in abilities to oxidation and the difference of particles of PdO and PtOx in affinity to SO_2 allow us to explain the high sulfur tolerance of the low Pt-loaded bimetallic catalyst. However, other reason needs to be looked for an explanation of great deactivation of the high Pt-loaded bimetallic catalyst.

PtO_x particles are known [75] to be prone to the sulfate-induced simultaneous reduction and sintering at elevated temperatures. Similarly to [31,90,92], increase of size of Pt as well as PtPd particles, and as a consequence a loss of catalytically active surface, can explain the observed deactivation of the high Pt-loaded bimetallic catalyst in the SO_2 presence. The decrease in the number of surface Pt atoms was detected by XPS as a drop of the surface Pt/Al ratio. The PtPd-alloy and Pt nanoparticles were found to catalyze oxidation of SO_2 to SO_3 [74,93], but they do not adsorb SO_3 [18]. For a Pt/alumina catalyst, sulfate ions are implied [75] to locate in the interface between Pt particles and alumina. We believe that the same interfacial sulfate ions form at the Pt and Mn-hexaaluminate interface. As a result, the Pt-highly-loaded bimetallic Mn-hexaaluminate catalyst deactivated under water and SO_2 presence is characterized by higher value of the surface S/Al ratio compared with other studied catalysts (XPS data, Table 2). Besides, PtPd-alloy nanoparticles, which is main active component in the Pt-highly-loaded bimetallic Mn-hexaaluminate catalyst, oxidize methane less efficiently compared with PdO and metal Pd [11,18,31].

Thus, when developing the bimetallic catalyst efficient in the oxidation of methane and stable in the presence of water vapor and SO_2 it is necessary to choose the best Pt/Pd ratio providing for the best content of non-crystalline catalytically active PdO particles and particles of a PtPd alloy stable in the presence of SO_2.

4. Conclusions

Water vapor has a weak deactivating effect on the catalytic activity of the unmodified and PtPd-modified Mn-hexaaluminate catalysts, whereas sulfur dioxide has a significant deactivating effect over the catalytic behavior of all studied catalysts, especially in the presence of water, with the only exclusion of PtPd(0.27)/$MnLaAl_{11}O_{19}$. Among the studied catalysts based on Mn-hexaaluminate, the latter is more resistant to the deactivation with water vapor and sulfur dioxide at 500 °C and higher.

The addition of Pt to the Pd-Mn-hexaaluminate catalyst up to the Pt/Pd atomic ratio close to 0.27 improves its stability in the methane oxidation in water and sulfur dioxide presence. There is also no decreasing of the high-temperature methane oxidation activity. Such performance of PtPd(0.27)/$MnLaAl_{11}O_{19}$ can be explained by the formation of both the PtPd alloy and PdO in the catalyst.

The HRTEM and H_2-TPR study of the Pd-Mn-hexaaluminate and Pt-doped catalysts showed that the positive effect on the methane oxidation activity is due to a highly dispersed PdO particles and PdO layer located on the surface of Pd^0. The presence of Mn^{3+} ions within $MnLaAl_{11}O_{19}$ also promotes a certain increase in the activity of the catalytic system. The catalytic activity of PtPd-$MnLaAl_{11}O_{19}$ is lowered, when there is a decrease in the share of non-crystalline and highly dispersed PdO particles due to an increase of platinum content in the catalysts above Pt/Pd = 0.3 as well as a sintering of the metal Pd particles under water vapor.

The PtPd-alloy formation that was observed in spite of PdO by H_2-TPR, HRTEM, and XPS in the catalyst with Pt/Pd = 0.27, correlates well with its high water and SO_2 tolerance, but features a lower activity in the oxidation of methane.

Sulfate-ion chemisorbs over the surface of the support, Mn-hexaaluminate. This assumption is confirmed by the IR-spectroscopy data, according to which the deactivated $MnLaAl_{11}O_{19}$, Pd/$MnLaAl_{11}O_{19}$ and PtPd/$MnLaAl_{11}O_{19}$ feature the absorption bands with nearly similar intensity at 1145 and 1065 cm^{-1} corresponding to the vibration of SO_4^{2-}-groups. Sulfate-ions in the deactivated catalysts are also registered with XPS, EDX, TG-DTA and H_2-TPR analyses. In the oxidizing conditions of TG-DTA, sulfate-ions are removed from the deactivated catalysts as SO_2 within 820–890 °C. In reducing conditions of the H_2-TPR experiments, sulfate-ions reduce to hydrogen sulfide and remove from the surface of deactivated catalysts at 540–600 °C. The additions of Pd and Pt to Mn-hexaaluminate promote the removal of sulfate-ions from the surface of the deactivated catalyst in both oxidizing and reducing conditions.

Acknowledgments

This work was partially supported by the Russian Foundation for Basic Research (Research project No. 15-03-05459-a). The authors thank A.A. Saraev for performing the XPS measurements, V.A. Ushakov for the XRD studies.

References

[1] S.H. Oh, P.J. Mitchell, R.M. Siewert, J. Catal. 132 (1991) 287–301.
[2] S.H. Oh, P.J. Mitchell, Appl. Catal. B 5 (1994) 165–179.
[3] R. Burch, P.K. Loader, Appl. Catal. B 5 (1994) 149–164.
[4] W.C. Pfefferle, L.D. Pfefferle, Prog. Energy Combust. Sci. 12 (1986) 25–41.
[5] Z.R. Ismagilov, M.A. Kerzhentsev, S.A. Yashnik, N.V. Shikina, A.N. Zagoruiko, V.N. Parmon, V.M. Zakharov, B.I. Braynin, O.N. Favorski, Development of granular catalysts and natural gas combustion technology for small gas turbine power plants, in: I. Gurrapa (Ed.), Gas Turbines, Sciyo, 2010, pp. 79–108 (Chapter 4).
[6] Z.R. Ismagilov, N.V. Shikina, S.A. Yashnik, A.N. Zagoruiko, S.R. Khairulin, M.A. Kerzhentsev, V.N. Korotkikh, V.N. Parmon, B.I. Braynin, V.M. Zakharov, O.N. Favorski, Kinet. Catal. 49 (2008) 873–886.
[7] S.A. Yashnik, N.V. Shikina, Z.R. Ismagilov, A.N. Zagoruiko, M.A. Kerzhentsev, V.N. Parmon, V.M. Zakharov, B.I. Braynin, O.N. Favorski, A.M. Gumerov, Catal. Today 147S (2009) 237–250.
[8] Z.R. Ismagilov, N.V. Shikina, S.A. Yashnik, A.N. Zagoruiko, M.A. Kerzhentsev, V.A. Ushakov, V.A. Sazonov, V.N. Parmon, V.M. Zakharov, B.I. Braynin, O.N. Favorski, Catal. Today 155 (2010) 35–44.
[9] Patent US 6015285, J.G. McCarty, V.L., Wong, B.J. Wood. Catalytic combustion process (2000).
[10] R.A. Dalla Betta, T. Rostrup-Nielsen, Catal. Today 47 (1999) 369–375.
[11] R. Burch, F.J. Urbano, Appl. Catal. A 124 (1995) 121–138.
[12] D. Ciuparu, N. Katsikis, L. Pfefferle, Appl. Catal. A 216 (2001) 209–215.
[13] D. Ciuparu, L. Pfefferle, Appl. Catal. A 209 (2001) 415–428.
[14] R. Burch, F.J. Urbano, P.K. Loader, Appl. Catal. A 123 (1995) 173–184.
[15] R. Burch, P.K. Loader, F.J. Urbano, Catal. Today 27 (1996) 243–248.
[16] F.H. Ribeiro, M. Chow, R.A. Dalla-Betta, J. Catal. 146 (1994) 537–544.
[17] R. Kikuchi, S. Maeda, K. Sasaki, S. Wennerstrom, K. Eguchi, Appl. Catal. A 232 (2002) 23–28.
[18] J.K. Lampert, M.S. Kazi, R.J. Farrauto, Appl. Catal. B 14 (1997) 211–223.
[19] T.-C. Yu, H. Shaw, Appl. Catal. B 18 (1998) 105–114.
[20] Y. Deng, T.G. Nevell, R.J. Ewen, C.L. Honeyboume, M.G. Jones, Appl. Catal. A 101 (1993) 51–62.
[21] L.J. Hoyos, H. Praliaud, M. Primet, Appl. Catal. A 98 (1993) 125–138.
[22] D.L. Mowery, M.S. Graboski, T.R. Ohno, R.L. McCormick, Appl. Catal. B 21 (1999) 157–169.
[23] D.L. Mowery, R.L. McCormick, Appl. Catal. B 34 (2001) 287–297.
[24] H.S. Gandhi, M. Shelef, Appl. Catal. 77 (1991) 175–186.
[25] P. Hurtado, S. Ordonez, H. Sastre, F.V. Diez, Appl. Catal. B 47 (2004) 85–93.
[26] F. Ortloff, J. Bohnau, U. Kramar, F. Graf, T. Kolb, Appl. Catal. B 182 (2016) 550–561.
[27] S.A. Yashnik, S.P. Denisov, N.M. Danchenko, Z.R. Ismagilov, Appl. Catal. B 21 (2016) 322–336.
[28] H.N. Rabinowitz, S.J. Tauster, R.M. Heck, Appl. Catal. A 212 (2001) 215–222.
[29] E.W. Qian, K. Otani, L. Li, A. Ishihara, T. Kabe, J. Catal. 221 (2004) 294–301.
[30] Y. Yoshimura, M. Toba, T. Matsui, M. Harada, Y. Ichihashi, K.K. Bando, H. Yasuda, H. Ishihara, Y. Morita, T. Kameoka, Appl. Catal. A 322 (2007) 152–171.
[31] G. Corro, C. Cano, J.L.G. Fierro, J. Mol. Catal. A 315 (2010) 35–42.
[32] H. Yamamoto, H. Uchida, Catal. Today 45 (1998) 147–151.
[33] K. Narui, H. Yata, K. Furuta, A. Nishida, Y. Kohtoku, T. Matsuzaki, Appl. Catal. A 179 (1999) 165–173.
[34] K. Persson, A. Ersson, K. Jansson, J.L.G. Fierro, S.G. Jaras, J. Catal. 243 (2006) 14–24.
[35] P. Castellazzi, G. Groppi, P. Forzatti, Appl. Catal. B 95 (2010) 303–311.
[36] K. Persson, A. Ersson, S. Colussi, A. Trovarelli, S.G. Jaras, Appl. Catal. B 66 (2006) 175–185.
[37] K. Persson, A. Ersson, A. Manrique Carrera, J. Jayasuriya, R. Fakhrai, T. Fransson, S. Jaras, Catal. Today 100 (2005) 479–483.
[38] Y. Ozawa, Y. Tochihara, A. Watanabe, M. Nagai, S. Omi, Appl. Catal. A 259 (2004) 1–7.
[39] K. Persson, L.D. Pfefferle, W. Schwartz, A. Ersson, S.G. Jaras, Appl. Catal. B 74 (2007) 242–250.
[40] S.A. Yashnik, Z.R. Ismagilov, V.V. Kuznetsov, V.V. Ushakov, V.A. Rogov, I.A. Ovsyannikova, Catal. Today 117 (2006) 525–535.
[41] S.A. Yashnik, Z.R. Ismagilov, Top. Catal. 55 (2012) 818–836.
[42] J.H. Scofield, J. Electron Spectrosc. Relat. Phenom. 8 (1976) 129–137.
[43] A.V. Matveev, V.V. Kaichev, A.A. Saraev, V.V. Gorodetskii, A. Knop-Gericke, V.I. Bukhtiyarov, B.E. Nieuwenhuys, Catal. Today 244 (2015) 29–35.
[44] M. Machida, K. Eguchi, H. Arai, J. Catal. 123 (1990) 477–485.
[45] W.R. Schwartz, D. Ciuparu, L.D. Pfefferle, J. Phys. Chem. C 116 (2012) 8587–8593.
[46] S.A. Yashnik, T.A. Surovtsova, A.V. Ishchenko, V.V. Kaichev, Z.R. Ismagilov, Kinet. Catal 57 (4) (2016) 528–539.
[47] M. Ferrandon, J. Carno, S. Jaras, E. Bjornbom, Appl. Catal. A 180 (1999) 153–161.
[48] J.V.D. Brand, P.C. Snijders, W.G. Sloof, H. Terryn, J.H.W.D. Wit, J. Phys. Chem. B 108 (2004) 6017–6024.
[49] V. Di Castro, G. Polzonetti, J. Electron Spectrosc. Relat. Phenom. 48 (1989) 117–123.
[50] C. Colmenares, S. Deutsch, C. Evans, A.J. Nelson, L.J. Terminello, J.G. Reynolds, J.W. Roos, I.L. Smith, Appl. Surf. Sci. 151 (1999) 189–202.
[51] J. Topfer, A. Feltz, D. Graf, B. Hackl, L. Raupach, P. Weissbrodt, Phys. Status Solidi A 134 (1992) 405–415.
[52] K. Otto, L.P. Haack, J.E. de Vries, Appl. Catal. B 1 (1992) 1–12.
[53] J.L. Hueso, A. Caballero, M. Ocana, A.R. Gonzalez-Elipe, J. Catal. 257 (2008) 334–344.
[54] T.L. Barr, J. Phys. Chem. 82 (1978) 1801–1810.
[55] P. Burroughs, A. Hamnett, A.F. Orchard, G. Thornton, Dalton Trans. J. Chem. Soc. 17 (1976) 1686–1698.
[56] D.P. Chzhu, P.G. Tsyrul'nikov, E.N. Kudrya, M.D. Smolikov, A.V. Bubnov, V.F. Borbat, Kinet. Cat. 43 (3) (2002) 379–383.
[57] Z. Xu, L. Zhao, F. Pang, L. Wang, C. Niu, J. Nat. Gas Chem. 16 (2007) 60–63.
[58] M.V. Bukhtiyarova, A.S. Ivanova, L.M. Plyasova, G.S. Litvak, V.A. Rogov, V.V. Kaichev, E.M. Slavinskaya, P.A. Kuznetsov, I.A. Polukhina, Appl. Catal. A 357 (2009) 193–205.
[59] J.S. Ledford, M. Houalla, A. Proctor, D.M. Gercules, L. Petrakis, J. Phys. Chem. 93 (1989) 6770–6777.

[60] G. Galtayries, G.A. Blanco, D. Cifredo, J.M. Finol, J.M. Gatica, H. Pintado, R. Vidal, S. Sporken, Bernal, Surf. Interface Anal. 27 (1999) 941–949.
[61] R.S. Monteiro, D. Zemlyanov, J.M. Storey, F.H. Ribeiro, J. Catal. 201 (2001) 37–45.
[62] K. Sun, W. Lu, M. Wang, X. Xu, Appl. Catal. A 268 (2004) 107–113.
[63] H.-P. Steinruck, F. Pesty, L. Zhang, T.E. Madey, Phys. Rev. B 51 (1995) 2427.
[64] G.M. Bancroft, I. Adams, L.L. Coatsworth, C.D. Bennewitz, J.D. Brown, W.D. Westwood, Anal. Chem. 47 (1975) 586–588.
[65] E.A. Anumol, A. Halder, C. Nethravathi, B. Viswanath, N. Ravishankar, J. Mater. Chem. 21 (2011), 8721–2826.
[66] S. Karthe, R. Szargan, E. Suoninen, Appl. Surf. Sci. 72 (1993) 157–170.
[67] N.H. Tran, R.N. Lamb, J. Phys. Chem. B 106 (2002) 352–355.
[68] K. Nakamoto, Infrared and Raman Spectra of Inorganic and Coordination Compounds, Moscow, Mir, 1991 [in Russian].
[69] T. Wang, A. Vazquez, A. Kato, L.D. Schmidt, J. Catal. 78 (1982) 306–318.
[70] A.M. Banerjee, M.R. Pai, R. Tewari, Naina Raje, A.K. Tripathi, S.R. Bharadwaj, D. Das, Appl. Catal. B: Environ. 162 (2015) 327–337.
[71] A.R. Powell, Platinum Met. Rev. 31 (2) (1958) 95–98.
[72] H.N. Sharma, V. Sharma, A.B. Mhadeshwar, R. Ramprasad, J. Phys. Chem. Lett. 6 (2015) 1140–1148.
[73] M. Happel, N. Luckas, F. Vines, M. Sobota, M. Laurin, A. Gorling, J. Libuda, J. Phys. Chem. C 115 (2011) 479–491.
[74] K. Wilson, C. Hardacre, R.M. Lambert, J. Phys. Chem 99 (1995) 13755–13758.
[75] A.F. Lee, K. Wilson, R.M. Lambert, C.P. Hubbard, R.G. Hurley, R.W. McCabe, H.S. Gandhi, J. Catal. 184 (1999) 491–498.
[76] J.H. Pazmino, J.T. Miller, S.S. Mulla, W.N. Delgass, F.H. Ribeiro, J. Catal. 282 (2011) 13–24.
[77] F. Kapteijn, D. van Langeveld, J.A. Moulijn, A. Andreini, M.A. Vuurman, A.M. Turek, J. Jehng, I.E. Wachs, J. Catal. 150 (1994) 94–104.
[78] R. Carroni, T. Griffin, Catal. Today 155 (2010) 2–12.
[79] S.C. Su, J.N. Carstens, A.T. Bell, J. Catal. 176 (1998) 125–135.
[80] R. Burch, Pure Appl. Chem. 68 (1996) 377–384.
[81] J.G. McCarty, Catal. Today 26 (1995) 283–293.
[82] H. Lieske, G. Lietz, H. Spindler, W. Hanke, J. Volter, J. Catal. 81 (1983) 17–25.
[83] H. Lieske, G. Lietz, H. Spindler, J. Volteri, J. Catal. 81 (1983) 8–16.
[84] H. Lieske, J. Volter, J. Phys. Chem. 89 (1985) 1841–1847.
[85] C. Hwang, C. Yeh, J. Mol. Catal. A 112 (1996) 295–302.
[86] W.S. Kijlstra, M. Biervliet, E.K. Poels, A. Bliek, Appl. Catal. B 16 (1998) 327–337.
[87] R.J. Farrauto, M.C. Hobson, T. Kennelly, E.M. Waterman, Appl. Catal. A 81 (1992) 227–237.
[88] J.N. Carstens, S.C. Su, A.T. Bell, J. Catal. 176 (1998) 136–142.
[89] P. Gelin, L. Urfels, M. Primet, E. Tena, Catal. Today 83 (2003) 45–57.
[90] R.F. Hicks, H. Qi, M.L. Young, R.G. Lee, J. Catal. 122 (1990) 280–294.
[91] K. Otto, J.M. Andino, C.L. Parks, J. Catal. 131 (1991) 243–251.
[92] T.F. Garetto, C.R. Apesteguia, Catal. Today 62 (2000) 189–199.
[93] S. Koutsopoulos, T. Johannessen, K.M. Eriksen, R. Fehrmann, J. Catal. 238 (2006) 206–213.